REFERENCES

Brown, A.S.C., Hargreaves, J.S.J., and Rijniersce, B. (1998). A study of the structural and catalytic effects of sulfation on iron oxide catalysts prepared from goethite and ferrihydrite precursors for methane oxidation. Catalysis Letters, 53, 7-13.

Brunner, T.J., Wick, P., Manser, P., Spohn, P., Grass, R.N., Limbach, L.K., Bruinink, A., and Stark, W.J. (2006). In vitro cytotoxicity of oxide nanoparticles: Comparison to asbestos, silica, and the effect of particle solubility. Environmental Science & Technology, 40, 43-74.

Bumajdad, A., Eastoe, J., Zaki, M.I., Heenan, R.K., and Pasupulety, L. (2007). Generation of metal oxide nanoparticles in optimised microemulsions. Journal of Colloid and Interface Science, 312, 68-75.

Cao, S., and Zhu, Y. (2008). Hierarchically nanostructured α-Fe_2O_3 hollow spheres: Preparation, growth mechanism, photocatalytic property, and application in water treatment. Journal of Physicl Chememistry C, 112, 6253-6257.

Cao, X., Prozorov, R., Koltypin, Y., Kataby, G., Felner, I., and Gedanken, A. (1997). Synthesis of pure amorphous Fe_2O_3. Journal of Materials Research, 12, 402-406.

Chauhan, P., Annapoomi, S., and Trikha, S.K. (1999). Humidity-sensing properties of nanocrystalline haematite thin films prepared by sol-gel processing. Thin Solid Films, 346, 266-268.

Chunhui, S., Mu, P., and Runzhang, Y. (2008). The effect of particle size gradation of conductive fillers on the conductivity and the flexural strength of composite bipolar plate. International Journal of Hydrogen Energy, 33, 1035-1039.

Cornell, R.M., and Giovanoli, R. (1985). Effect of solution conditions on the proportion and morphology of goethite formed from ferrihydrite. Clays and Clay Minerals, 33, 424-432.

Cornell, R.M., and Schwertmann, U. (1996). The Iron Oxides: Structure, Properties, Reaction, Occurrences and Uses. Weinheim: Wiley-VCH.

Cornell, R.M., and Schwertmann, U. (2003). The Iron Oxides: Structure, Properties, Reaction, Occurrences and Uses. Weinheim: Wiley-VCH.

Dave, S.R., and Gao, X. (2009). Monodisperse magnetic nanoparticles for biodetection, imaging, and drug delivery: A versatile and evolving technology. Nanobiotechnol, 1, 583-609.

De Yoreo, J.J., and Vekilov, P.G. (2003). Principles of crystal nucleation and growth. Reviews in Mineralogy and Geochemistry, 54, 57-93.

Diamandescu, L., Mihaila-Tarabasanu, D., Popescu-Pogrion, N., Totovina, A., and Bibicu, I. (1999). Hydrothermal synthesis and characterization of some polycrystalline α-iron oxides. Ceramics International, 25, 689-692.

Greedon, J.E. (1994). Magnetic Oxides in Encyclopedia of Inorganic Chemistry. Bruce King: John Wiley & Sons.

Han, L.-H., Liu, H., and Wei, Y. (2011). In situ synthesis of hematite nanoparticles using a low-temperature microemulsion method. Powder Technology, 207, 42-46.

Han, M.G., and Armes, S.P. (2003). Synthesis of poly(3,4-ethylenedioxythiophene)/ silica colloidal nanocomposites. Langmuir, 19, 4523-4526.

Hu, X., and Yu, J.C. (2008). Continuous aspect-ratio tuning and fine shape control of monodisperse α-Fe_2O_3 nanocrystals by a programmed microwave-hydrothermal method. Advanced Functional Materials, 18, 880-887.

Huang, Z., Feng, Q., Chen, Z., Chen, S., and Du, Y. (2003). Surface and size effects of magnetic properties in ferromagnetic nanoparticles. Microelectronic Engineering, 66, 128-135.

Huo, L., Li, W., Lu, L., Cui, H., Xi, S., Wang, J., Zhao, B., Shen, Y., and Lu, Z. (2000). Preparation, structure, and properties of three-dimensional ordered α-Fe_2O_3 nanoparticulate film. Chemistry of Materials, 12, 790-794.

Jing, Z., and Wu, S. (2004). Synthesis and characterization of monodisperse hematite nanoparticles modified by surfactants via hydrothermal approach. Materials Letters, 58, 3637-3640.

Kacprzak, D. (2001). Electeng 204 Lec Engineering Electromagnetics. New Zealand: University of Auckland.

Kandori, K., Ohnishi, S., Fukusumi, M., and Morisada, Y. (2008). Effects of anions on the morphology and structure of hematite particles produced from forced hydrolysis of $Fe(NO_3)_3$–HNO_3. Colloids and Surfaces A: Physicochemical and Engineering Aspects, 331, 232-238.

Kay, A., Cesar, I., and Gratzel, M. (2006). New benchmark for water photooxidation by nanostructured α-Fe_2O_3 films. Journal of American Chemical Society, 128, 15714-15721.

Larson, B. (2006). Introduction to Magnetic Particle Inspection: The Hysteresis Loop and Magnetic Properties. USA: Iowa State University.

Li, L., Li, G., Smith R.L. Jr., and Inomata, H. (2000). Microstructural evolution and magnetic properties of $NiFe_2O_4$ nanocrystals dispersed in amorphous silica. Chemistry of Materials, 12, 3705-3714.

Lian, J., Duan, X., Ma, J., Peng, P., Kim, T., and Zheng, W. (2009). Hematite (α-Fe_2O_3) with various morphologies: Ionic liquid-assisted synthesis, formation mechanism, and properties. ACS Nano, 3, 3749-3761.

Lian, S., Wang, E., Kang, Z., Bai, Y., Gao, L., Jiang, M., Hu, C., and Xu, L. (2004). Synthesis of magnetite nanorods and porous hematite nanorods. Solid State Communications, 129, 485-490.

Liu, H., Li, P., Lu, B., Wei, Y., and Sun, Y. (2009). Transformation of ferrihydrite in the presence and absence of trace Fe(II): The effect of preparation procedure of ferrihydrite. Journal of Solid State Chemistry, 182, 1767-1771.

Liu, H., Ma, M., Qin, M., Yang, L., and Wei, Y. (2010). Studies on the controllable transformation of ferrihydrite. Journal of Solid State Chemistry, 183, 2045-2050.

Liu, H., Wei, Y., and Sun, Y. (2005). The formation of hematite from ferrihydrite using Fe(II) as a catalyst. Journal of Molecular Catalysis A: Chemical, 226, 135-140.

Liu, H., Wei, Y., Li, P., Zhang, Y., and Sun, Y. (2007). Catalytic synthesis of nanosized hematite particles in solution. Materials Chemistry and Physics, 102, 1-6.

Liu, X., Fu, S., Xiao, H., and Huang, C. (2005). Preparation and characterization of shuttle-like α-Fe_2O_3 nanoparticles by supermolecular template. Journal of Solid State Chemistry, 178, 2798-2803.

Lu, J., Chen, D., and Jiao, X. (2006). Fabrication, characterization, and formation mechanism of hollow spindle-like hematite via a solvothermal process. Journal of Colloid and Interface Science, 303, 437-443.

Machala, L., Tucek, J., and Zboril, R. (2011). Polymorphous transformations of nanometric iron(III) oxide: A review. Chemistry of Materials, 23, 3255-3272.

Mercier, J.P., Zambelli, G., and Kurz, W. (2002). Introduction to Materials Science. Netherlands: Elsevier.

Min, C., Huang, Y., and Liu, L. (2007). High-yield synthesis and magnetic property of hematite nanorhombohedras through a facile solution route. Materials Letters, 61, 4756-4758.

Music, S., Krehula, S., Popovic, S., and Skoko, Z. (2003). Some factors influencing forced hydrolysis of $FeCl_3$ solutions. Materials Letters, 57, 1096-1102.

Nassar, N., and Husein, M. (2006). Preparation of iron oxide nanoparticles from $FeCl_3$ solid powder using microemulsions. Physca Status Solidi, 203, 1324-1328.

Ocana, M., Morales, M.P., and Cerna, C.J. (1995). The growth mechanism of α-Fe_2O_3 ellipsoidal particles in solution. Journal of Colloid and Interface Science, 171, 85-91.

Petcharoen, K., and Sirivat, A. (2012). Synthesis and characterization of magnetite nanoparticles via the chemical co-precipitation method. Materials Science and Engineering B, 177, 421-427.

Raming, T.P., Winnubst, A.J.A., van Kats, C.M., and Philipse, A.P. (2002). The synthesis and magnetic properties of nanosized hematite (α-Fe_2O_3) particles. Journal of Colloid and Interface Science, 249, 346-350.

Ristic, M., De Grave, E., Music, S., Popovic, S., and Orehovec, Z. (2007). Transformation of low crystalline ferrihydrite to α-Fe_2O_3 in the solid state. Journal of Molecular Structure, 834, 454-460.

Sarangi, P.P., Vadera, S.R., Patra, M.K., Prakash, C., and Ghosh, N.N. (2009). DC electrical resistivity and magnetic property of single-phase α-Fe_2O_3 nano-

powder synthesized by a simple chemical method. Journal of American Ceramic Society, 92, 2425-2428.

Schwertmann, U., and Cornell, R.M. (2000). Iron Oxides in the Laboratory Preparation and Characterization. Weinheim: Wiley-VCH.

Schwertmann, U., Friedl, J., and Stanjek, H. (1999). From Fe(III) Ions to ferrihydrite and then to hematite. Journal of Colloid and Interface Science, 209, 215-223.

Spaldin, N.A. (2003). Magnetic Materials: Fundamentals and Device Applications. UK: University of Cambridge.

Su, C., Wang, H., and Liu, X. (2011). Controllable fabrication and growth mechanism of hematite cubes. Crystal Research and Technology, 46, 209-214.

Sun, Q., Lu, X., and Liang, G. (2010). Controlled template-free hydrothermal synthesis of hematite nanoplatelets. Materials Letters, 64, 2006-2008.

Tang, B., Wang, G., Zhuo, L., Ge, J., and Cui, L. (2006). Facile route to α-FeOOH and α-Fe_2O_3 nanorods and magnetic property of α-Fe_2O_3 nanorods. Inorganic Chemistry, 45, 5196-5200.

Teja, A.S., and Koh, P.-Y. (2009). Synthesis, properties, and applications of magnetic iron oxide nanoparticles. Progress in Crystal Growth and Characterization of Materials, 55, 22-45.

Vatta, L.L., Sanderson, R.D., and Koch, K.R. (2006). Magnetic nanoparticles: Properties and potential applications. Pure and Applied Chemistry, 78, 1793-1801.

Wang, D., Cao, C., Xue, S., and Zhu, H. (2005). γ-Fe_2O_3 oriented growth by surfactant molecules in microemulsion. Journal of Crystal Growth, 277, 238-245.

Wang, L., and Jiang. T. (2009). Preparation of Fe_3O_4 spherical nanoporous particles facilitated by polyethylene glycol 4000. Nanoscale Research Letters, 4, 1439-1446.

Watanabe, A., and Kozuka, H. (2003). Photoanodic properties of sol-gel-derived Fe_2O_3 thin films containing dispersed gold and silver particles. Journal of Physical Chemistry B, 107, 12713-12720.

Wu, Z., Yu, K., Zhang, S., and Xie, Y. (2008). Hematite hollow spheres with a mesoporous shell: Controlled synthesis and applications in gas sensor and lithium ion batteries. Journal of Physical Chemistry C, 112, 11307-11313.

Zhang, Y.C., Tang, J.Y., and Hu, X.Y. (2008). Controllable synthesis and magnetic properties of pure hematite and maghemite nanocrystals from a molecular precursor. Journal of Alloys and Compounds, 462, 24-28.

Zysler, R.D., Mansilla, M.V., and Fiorani, D. (2004). Surface effects in α-Fe_2O_3 nanoparticles. European Physical Journal B, 41, 171-175.

APPENDICES

Appendix A Amounts of Chemicals Used to Synthesize Hematite Particles and Yield Percentage of the Products

Table A1 Properties of the chemicals used in the experiment

Chemicals	Molecular formula	Molecular weight (g/mol)	Appearance	Solubility
Ferric chloride anhydrous	$FeCl_3$	162.21	dark green powder	Easily soluble in cold, hot water
Ferrous chloride tetrahydrate	$FeCl_2{\cdot}4H_2O$	198.81	light yellow powder	Easily soluble in cold water
Sodium hydroxide	NaOH	40.00	white pellet	Easily soluble in cold water
Ammonia solution	$NH_3{\cdot}H_2O$	17.03	clear solution	Completely soluble in water
Sodium chloride	NaCl	58.44	white powder	Easily soluble in cold, hot water

Table A2 Amounts of chemicals used to synthesize hematite particles at various precursor concentrations with the constant $n_{Fe(II)}/n_{Fe(III)} = 0.02$, pH 7, 100 °C, and 1h

Precursor conc.(M)	50 ml Fe(III) conc.(M)	Fe(II) weight(g)	6.0 M NaOH volume(ml)	1.0 M NaOH volume(ml)	Distilled water volume(ml)
0.1	0.2	0.0398	5.0	0.4	44.6
0.2	0.4	0.0795	10.0	0.8	39.2
0.3	0.6	0.1193	15.0	1.2	33.8
0.4	0.8	0.1590	20.0	1.6	28.4
0.5	1.0	0.1988	25.0	2.0	23.0

Table A3 Amounts of chemicals used to synthesize hematite particles at various precursor concentrations (dilution method) with the constant $n_{Fe(II)}/n_{Fe(III)} = 0.02$, pH 7, 100 °C, and 1h

Precursor conc. (M)	1.0M Fe(III) + water vol. (ml)	6.0M NaOH vol. (ml)	Fe(II) wt. (g)	1.0M NaOH vol. (ml)	Distilled water vol. (ml)
0.1	25.0 + 100	12.5	0.099405	1.0	111.5
0.2	25.0 + 37.5	12.5	0.099405	1.0	49.0
0.3	25.0 + 16.6	12.5	0.099405	1.0	28.2
0.4	25.0 + 6.25	12.5	0.099405	1.0	17.75
0.5	25.0 + 0	12.5	0.099405	1.0	11.5

Table A4 Amounts of chemicals used to synthesize hematite particles at various solution pHs with the constant $C = 0.3$ M, $n_{Fe(II)}/n_{Fe(III)} = 0.02$, 100 °C, and 1h

Solution pH	1.0M Fe(III) + water vol. (ml)	6.0M NaOH vol. (ml)	Fe(II) wt. (g)	1.0M NaOH vol. (ml)	Distilled water vol. (ml)
pH 5	25.0 + 16.6	12.5	0.0994	0	29.2
PH 6	25.0 + 16.6	12.5	0.0994	1.0	28.2
pH 7	25.0 + 16.6	12.5	0.0994	2.0	27.2
pH 8	25.0 + 16.6	12.5	0.0994	3.0	26.2
pH 9	25.0 + 16.6	12.5	0.0994	3.5	25.7

Table A5 Amounts of chemicals used to synthesize hematite particles at various amounts of Fe(II) with the constant C = 0.3 M, pH 7, 100 °C, and 1h

$n_{Fe(II)}/n_{Fe(III)}$	1.0M Fe(III) + water vol. (ml)	6.0M NaOH vol. (ml)	Fe(II) wt. (g)	1.0M NaOH vol. (ml)	Distilled water vol. (ml)
0.01	25.0 + 16.6	12.5	0.0497	0.5	28.7
0.02	25.0 + 16.6	12.5	0.0994	1.0	28.2
0.03	25.0 + 16.6	12.5	0.1491	1.5	27.7
0.04	25.0 + 16.6	12.5	0.1988	2.0	27.2
0.05	25.0 + 16.6	12.5	0.2485	2.5	26.7

Table A6 Amounts of chemicals used to synthesize hematite particles at various ionic strength (I) values with the constant C = 0.3 M, $n_{Fe(II)}/n_{Fe(III)}$ = 0.02, pH 7, 100 °C, and 1h

I (M)	1.0M Fe(III) + water vol. (ml)	6.0M NaOH vol. (ml)	Fe(II) wt. (g)	1.0M NaOH vol. (ml)	5.0M NaCl vol. (ml)	Distilled water vol. (ml)
1.0	25.0 + 16.6	12.5	0.0994	1.0	1.5	26.7
1.2	25.0 + 16.6	12.5	0.0994	1.0	4.8	23.4
1.4	25.0 + 16.6	12.5	0.0994	1.0	8.1	20.0
1.6	25.0 + 16.6	12.5	0.0994	1.0	11.5	16.7
1.8	25.0 + 16.6	12.5	0.0994	1.0	14.8	13.4
2.0	25.0 + 16.6	12.5	0.0994	1.0	18.1	10.0

Note: The ionic strength (I) of the solution is calculated from equation (A1) as follow:

$$I = \sum_{i=1}^{n} C_i \, Z_i^2 \qquad \text{(A1)}$$

where I = ionic strength (mol/L)

C_i = molar concentration of each individual ion in the solution (mol/L)

Z_i = valence of each individual ion in the solution

Table A7 Summary of yield percentage (%) of the synthesized hematite particles at various precursor concentrations with the constant $n_{Fe(II)}/n_{Fe(III)} = 0.02$, pH 7, 100 °C, and 1h

Sample	Calculated weight (g)	Sample weight (g)	Yield percentage (%)
Hematite $C = 0.05$ M	0.3992	0.1425	35.7
Hematite $C = 0.1$ M	0.7985	0.4862	60.9
Hematite $C = 0.2$ M	1.5969	1.2484	78.2
Hematite $C = 0.3$ M	2.3954	1.9968	83.4
Hematite $C = 0.4$ M	3.1938	2.7951	87.5
Hematite $C = 0.5$ M	3.9923	3.5689	89.4

Appendix B XRD Patterns of the Synthesized Hematite Nanoparticles

A powder X-ray diffractometer (Bruker AXS, D8 Advance) was used to examine the crystal structure of the synthesized hematite particles which were below the nanometer scale. The Cu Kα (λ = 1.5406 Å) radiation source was operated at 40 kV/30 mA and used the Kβ filter to eliminate the interference peak. Divergence slit and scattering slit 0.5 deg together with 0.3 mm of receiving slit were set on the instrument. The hematite powder was placed into a sample holder and the measurement was continuously run. The experiments were recorded by monitoring the diffraction in the diffraction angle (2θ) range from 10.000 to 80.000 deg with a scan speed of 1.000 deg/min and a scan step of 0.020 deg.

The crystallite sizes of the synthesized hematite nanoparticles could be estimated from the XRD patterns by using Scherrer's equation (B1) as follow:

$$D = \frac{k\lambda}{\beta \cos\theta} \tag{B1}$$

where D = crystallite size (nm)

k = grain shape dependent constant (assumed to be 0.89 for the spherical particles)

λ = wave length of X-ray beam (nm) (λ = 0.15406 nm for Cu Kα radiation)

β = full width at half maximum (FWHM) for the considered diffraction peak (rad)

θ = diffraction angle (°)

Note: For hematite, the crystallite sizes calculated from (104) diffraction peak located at $2\theta = 33.2°$

Table B1 Summary of the estimated crystallite sizes of the synthesized hematite nanoparticles from the XRD patterns using Scherrer's equation

Sample	104 peak (°)	FWHM (°)	Crystallite size (nm)
Hematite C = 0.1 M	33.168	0.403	20.3
Hematite C = 0.3 M	33.230	0.245	33.5
Hematite C = 0.5 M	33.238	0.203	40.4

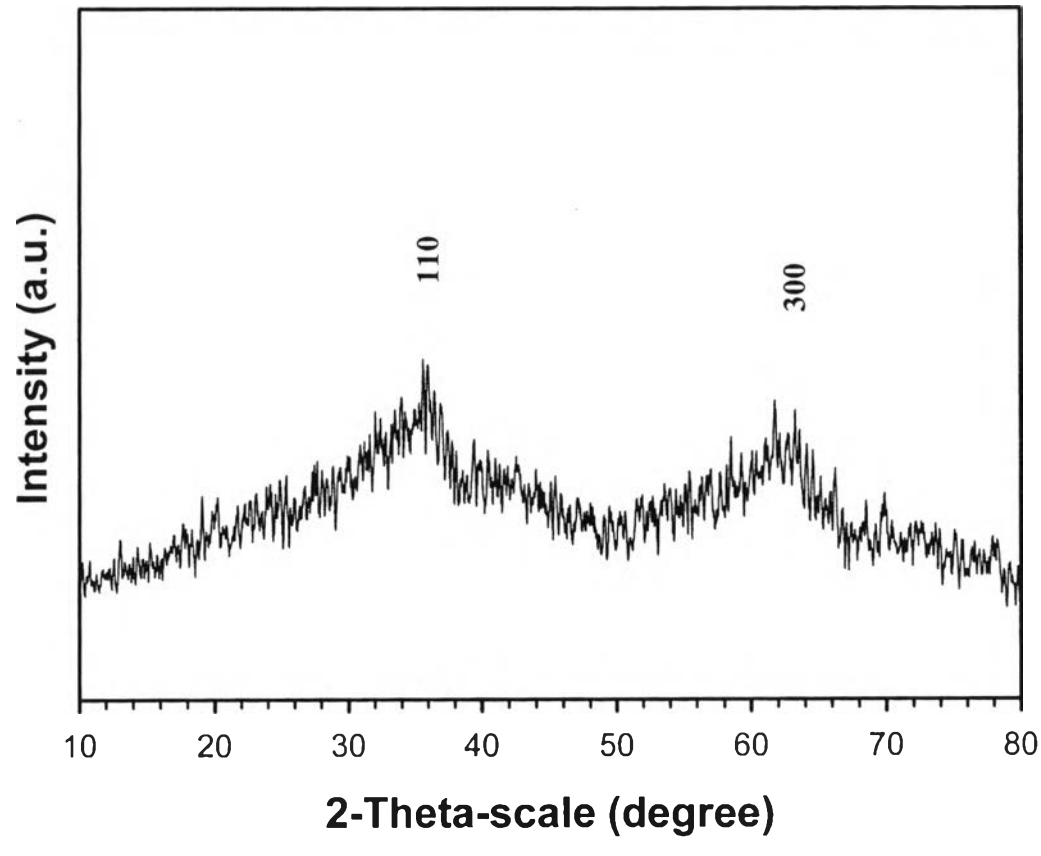

Figure B1 XRD pattern of the 2-line ferrihydrite precursor (C = 0.3 M, and pH 7).

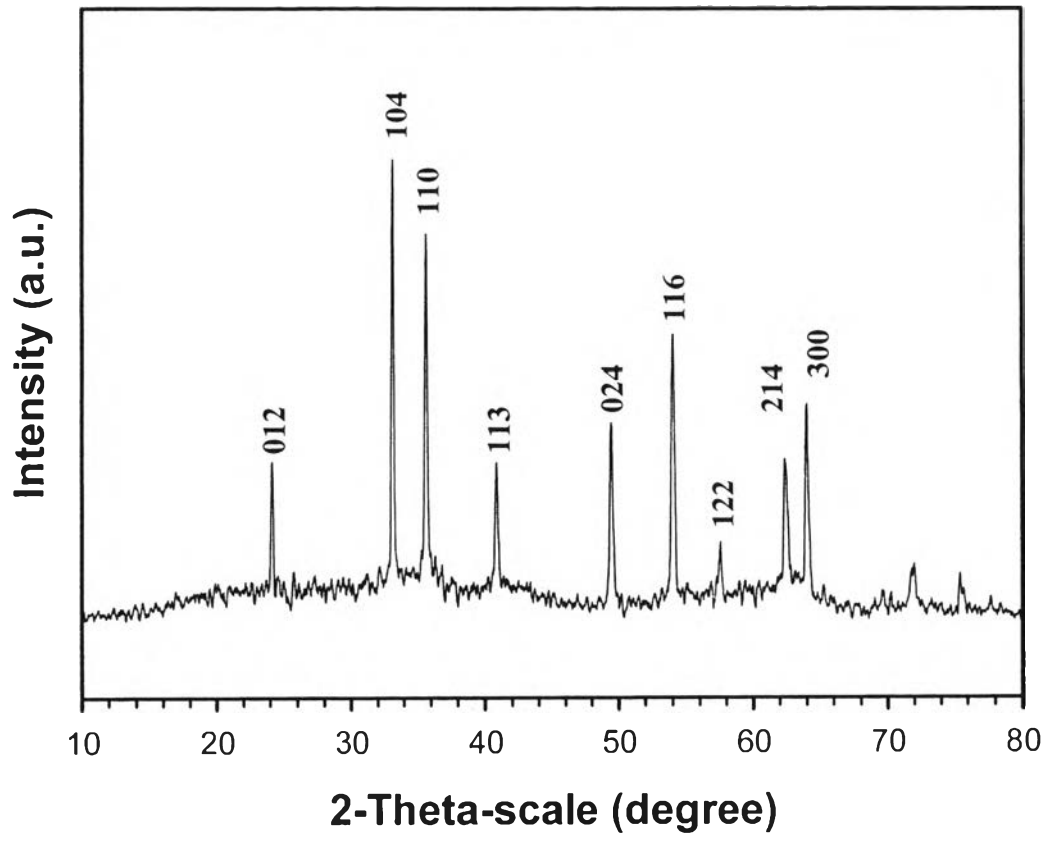

Figure B2 XRD pattern of the synthesized hematite nanoparticles (C = 0.1 M, $n_{Fe(II)}/n_{Fe(III)}$ = 0.02, pH 7, 100 °C, and 1h).

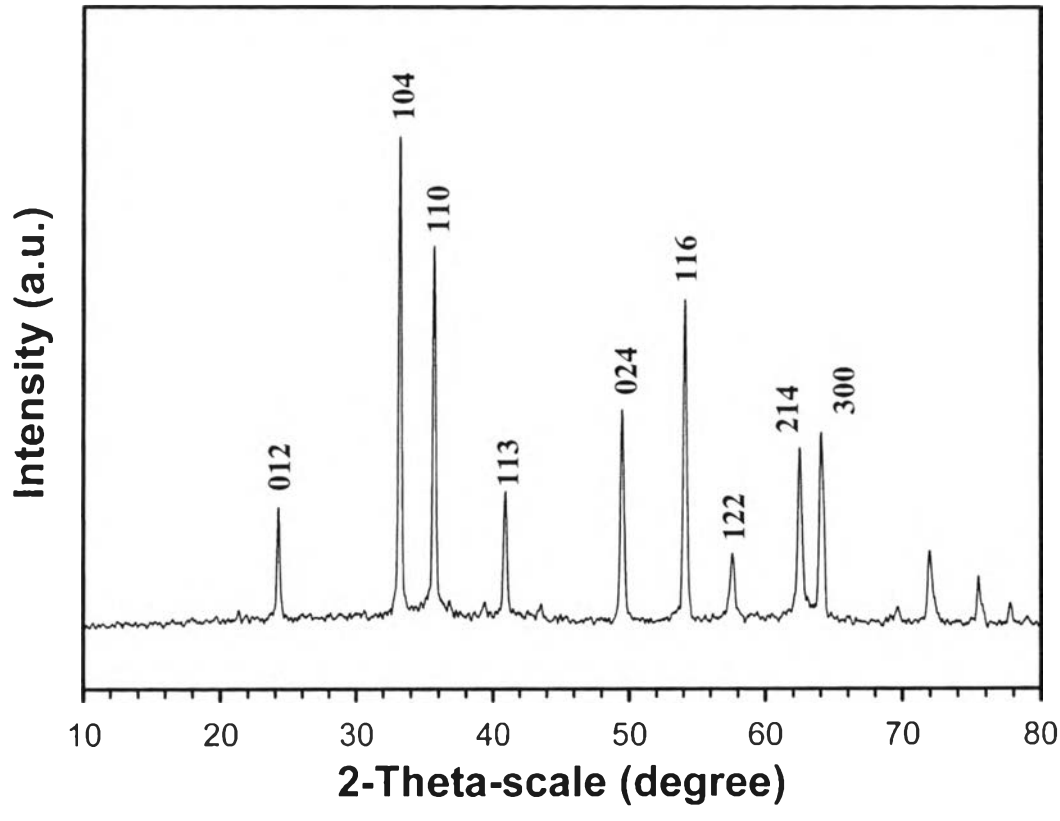

Figure B3 XRD pattern of the synthesized hematite nanoparticles (C = 0.3 M, $n_{Fe(II)}/n_{Fe(III)}$ = 0.02, pH 7, 100 °C, and 1h).

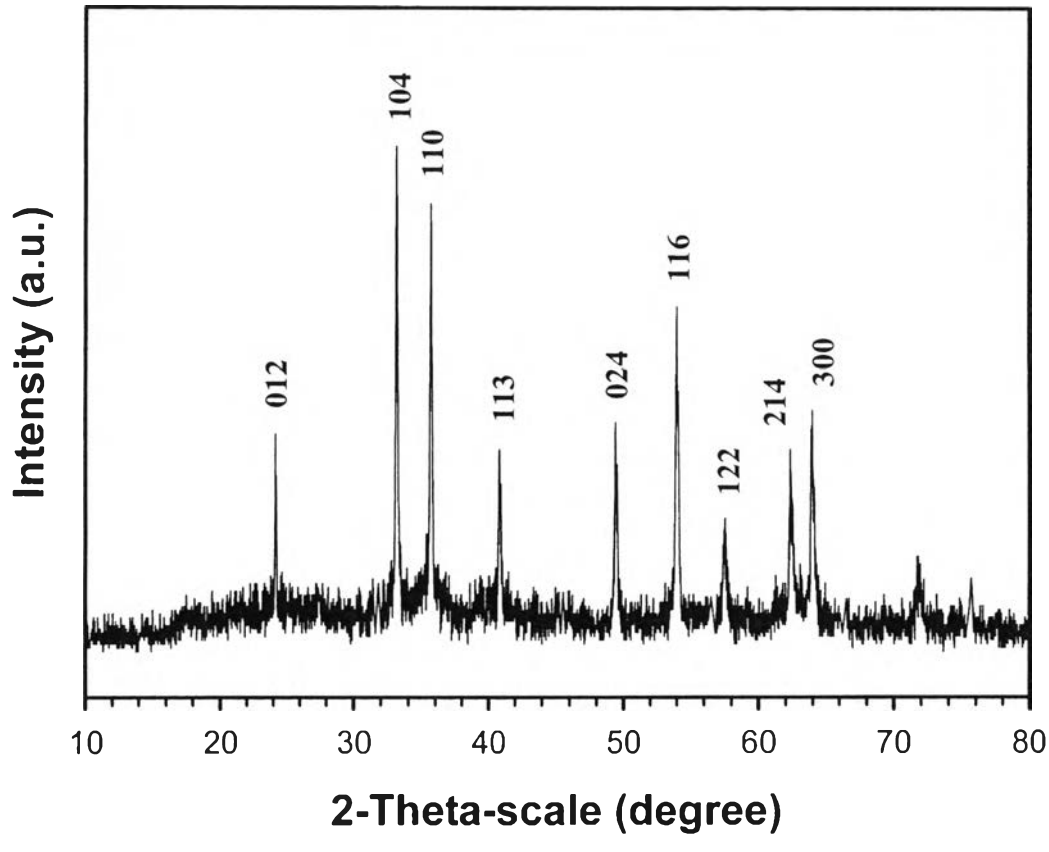

Figure B4 XRD pattern of the synthesized hematite nanoparticles (C = 0.5 M, $n_{Fe(II)}/n_{Fe(III)}$ = 0.02, pH 7, 100 °C, and 1h).

Table B2 Powder X-ray diffraction data of ferrihydrite and hematite (Joint Committee on Powder Diffraction Standard; JCPDS) (adapted from Cornell and Schwertmann, 2003)

Ferrihydrite ($Fe_5HO_8 \cdot 4H_2O$)				**Hematite (α-Fe_2O_3)**			
2θ (°)	*I*	*hkl*	*d* (nm)	2θ (°)	*I*	*hkl*	*d* (nm)
35.452	100	110*	0.250	24.033	30	012	0.3684
39.920	80	112	0.221	33.027	100	104	0.2700
45.505	80	113	0.196	35.452	70	110	0.2591
52,579	50	114	0.172	40.798	20	113	0.2207
60.771	70	115	0.151	49.212	40	024	0.1841
62.260	80	300*	0.148	53.888	45	116	0.1694
				57.168	10	122	0.1599
Note: There are two types of ferrihydrite: 2-line ferrihydrite; and 6-line ferrihydrite (the stars (*) are assigned to peaks of 2-line ferrihydrite).				62.260	30	214	0.1486
				63.687	30	300	0.1454
				71.403	10	$10\underline{1}0$	0.1312
				74.679	8	220	0.1259

Note: 2θ is the diffraction angle (°); *I* is the relative intensity; *hkl* is the Miller indices; and *d* is the spacing between the adjacent (*hkl*) lattice planes (nm).

Appendix C FT-IR Spectra of the Synthesized Hematite Nanoparticles

A Fourier transform infrared spectrometer (Thermo Nicolet, Nexus 670), with a deuterated triglycine sulfate detector, was used to characterize the functional groups of the synthesized hematite particles. For the KBr-pellet technique, optical grade KBr (Carlo Erba Reagent) was used as the background material. The hematite powder was grounded in a motar and mixed with dried KBr at ratio of the sample:KBr was about 1:20, then the mixed powder was compressed into the pellets under the pressure of 7 tons. The absorption mode was run 64 scans with a resolution of ± 4 cm^{-1} in the wave number in range of 4000-400 cm^{-1}.

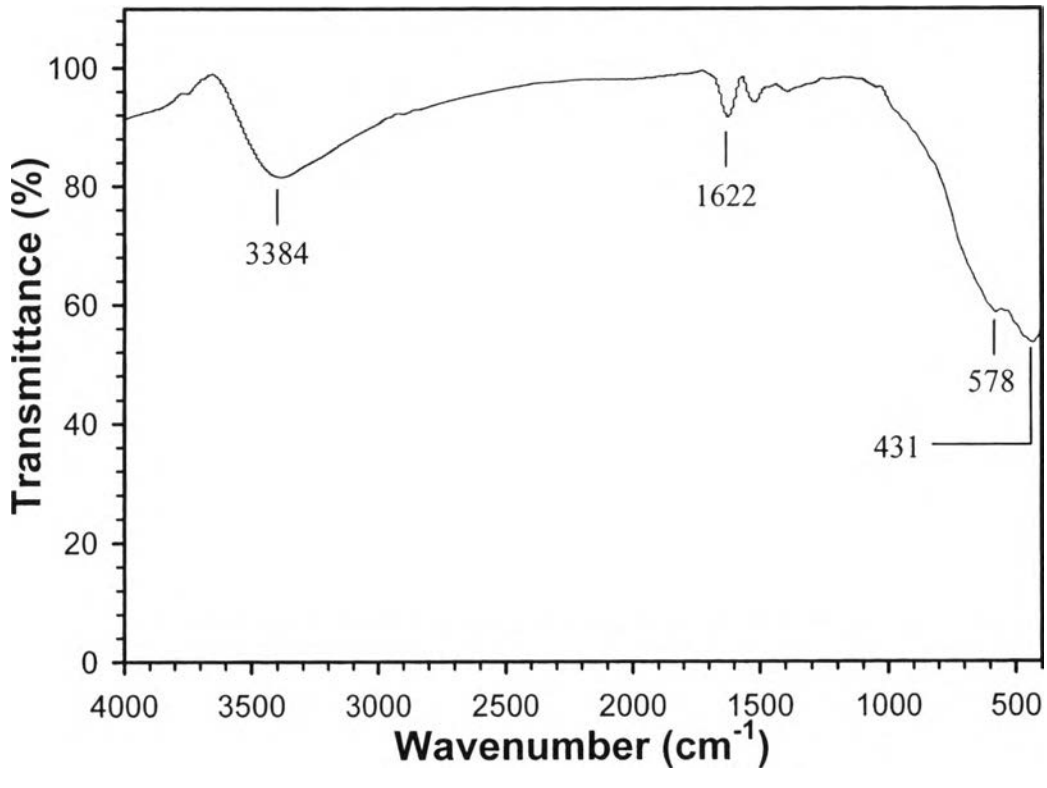

Figure C1 FT-IR spectrum of the 2-line ferrihydrite precursor (*C*=0.3 M, and pH 7).

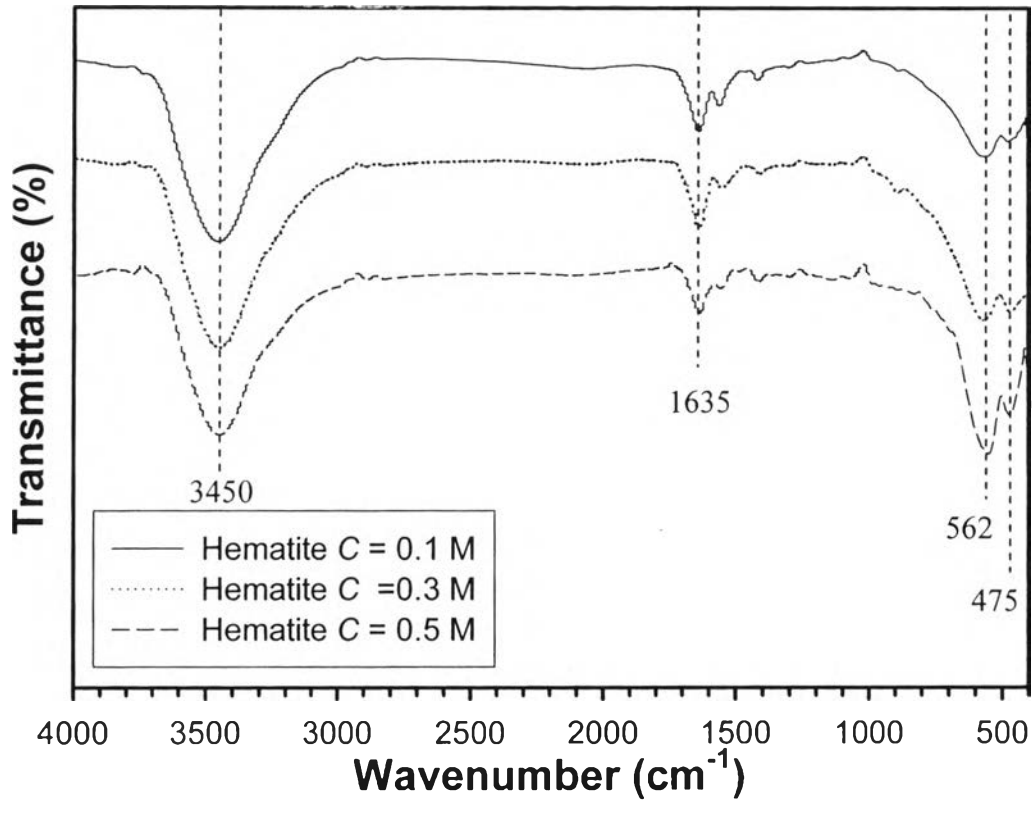

Figure C2 FT-IR spectra of the synthesized hematite nanoparticles ($n_{Fe(II)}/n_{Fe(III)}$ = 0.02, pH 7, 100 °C, and 1h).

Table C1 Summary of FT-IR bands of the 2-line ferrihydrite precursor and the synthesized hematite nanoparticles

Sample	Observed wavenumbers (cm^{-1})	
	Adsorbed water	**Fe-O bond**
2-line ferrihydrite	3384 and 1621	577 and 430
Hematite *C* = 0.1 M	3452 and 1638	567 and 477
Hematite *C* = 0.3 M	3448 and 1637	569 and 472
Hematite *C* = 0.5 M	3449 and 1632	560 and 475

Table C2 Peak positions for IR bands of ferrihydrite and hematite

Sample	**Functional groups**	**Wavenumbers (cm^{-1})**	**References**
Ferrihydrite ($Fe_5HO_8 \cdot 4H_2O$)	Adsorbed or lattice water (stretching and bending vibration of water molecules)	3357 and 1622	(Ristic *et al.*, 2007)
		~3400 and ~1600	(Liu *et al.*, 2009)
	Fe-O bond	580 and 441	(Ristic *et al.*, 2007)
		~585 and ~459	(Liu *et al.*, 2009)
Hematite (α-Fe_2O_3)	Adsorbed water (stretching and bending vibration of water molecules)	3420 and 1635	(Jing and Wu, 2004)
		3359.8 and 1616.2	(Liu *et al.*, 2007)
	Fe-O bond	560 and 479	(Jing and Wu, 2004)
		578.6 and 474.3	(Liu *et al.*, 2007)

Appendix D TG/DTA Curves of the Synthesized Hematite Nanoparticles

A thermogravimetric/differential thermal analyzer (Perkin Elmer, Pyris Diamond) was used to determine the thermal behaviour of the synthesized hematite particles. The experiment was carried out by weighting a powder sample of 1-5 mg and loaded into a platinum pan. The mass change under the temperature scan from 30 to 600 °C at a heating rate of 10 °C/min and under the nitrogen flow was monitored and recorded.

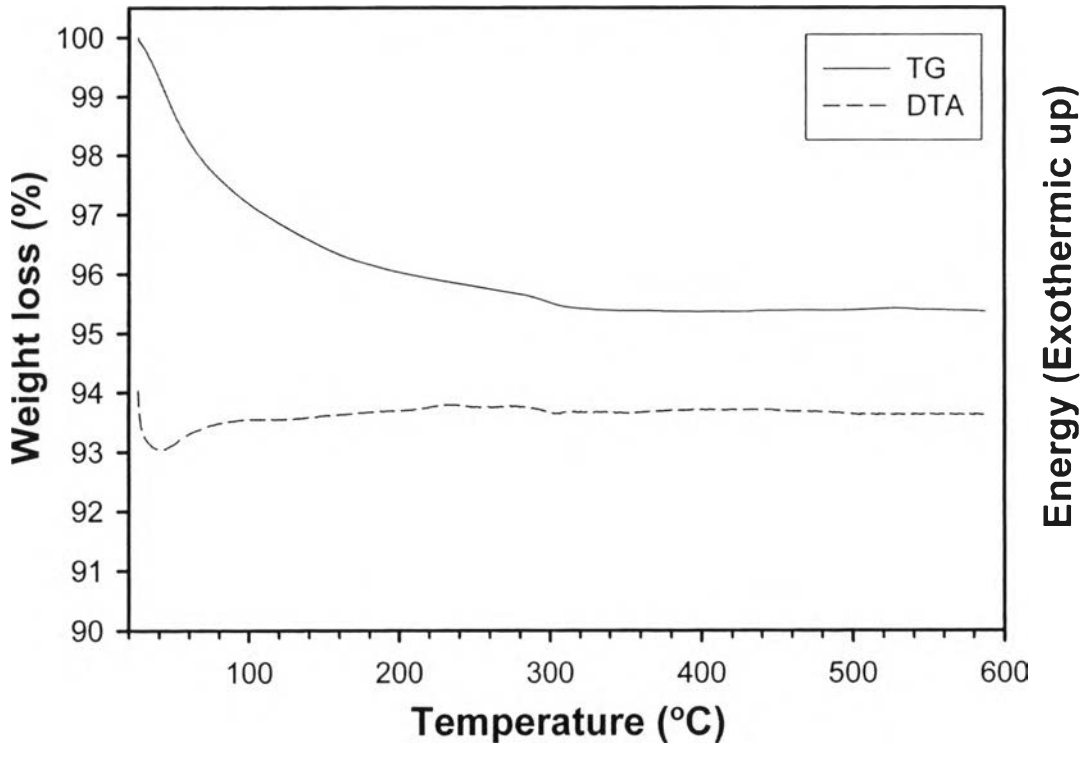

Figure D1 TG-DTA curves of the synthesized hematite nanoparticles (C = 0.3 M, $n_{Fe(II)}/n_{Fe(III)}$ = 0.02, pH 7, 100 °C, and 1h).

Table D1 Thermal behavior assignations for TG/DTA curves of hematite

Mode	Behavior	Temperature (°C)	References
DTA	Endothermic peak (elimination of adsorbed water on the surface)	25-50	(Kandori *et al.*, 2008)
TG	Mass loss about 4.0 % (removal of adsorbed water)	below 200	(Lu *et al.*, 2006)
	Mass loss about 0.5 % (elimination of hydroxyl group)	200-400	(Lu *et al.*, 2006)

Appendix E FE-SEM Images of the Synthesized Hematite Nanoparticles

A field-emission scanning electron microscope (Hitachi, S-4800) was used to examine the morphological structure and to determine the particle size of the synthesized hematite particles. The sample powder was placed on the holder with an adhesive tape and coated with a thin layer of platinum using an ion sputtering device (Hitachi, E-1010) for 100 sec prior to observation under FE-SEM. The scanning electron images were investigated by using an acceleration voltage of 5.0 kV with a magnification in the range of 50.0-200k times.

Table E1 Summary of FE-SEM images of the 2-line ferrihydrite precursor and the synthesized hematite nanoparticles with different morphologies

Sample	FE-SEM images	
	Low magnification (50kX)	High magnification (100kX)
Ferrihydrite	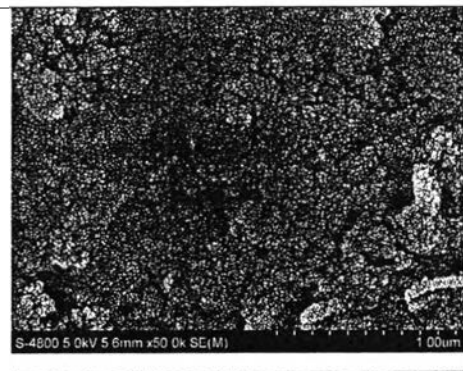	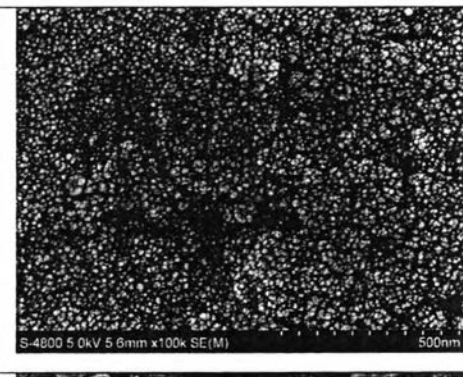
Spherical hematite	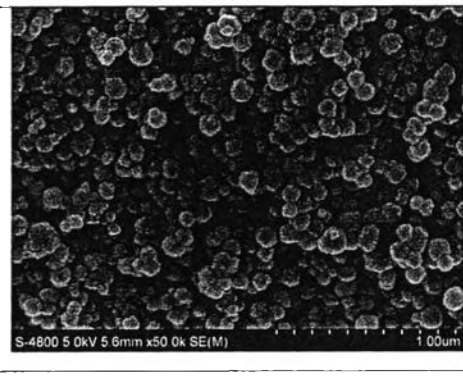	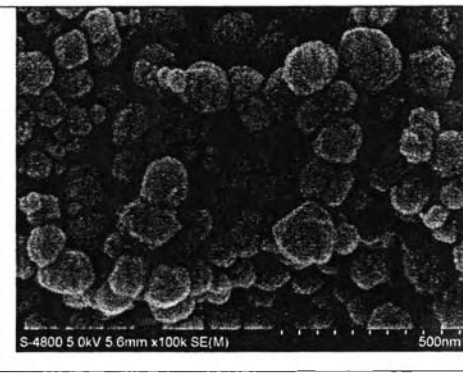

Sample	FE-SEM images	
	Low magnification (50kX)	High magnification (100kX)
Cubic hematite	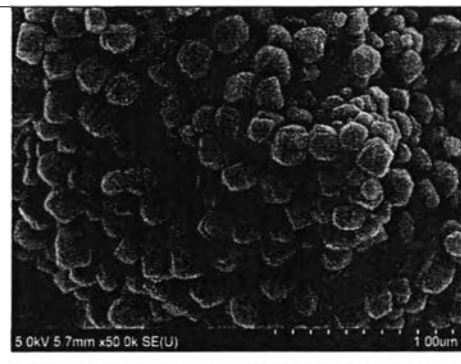	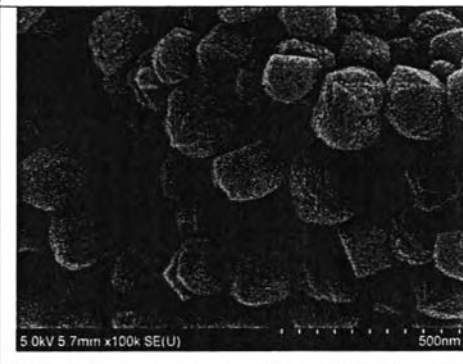
Ellipsoidal hematite	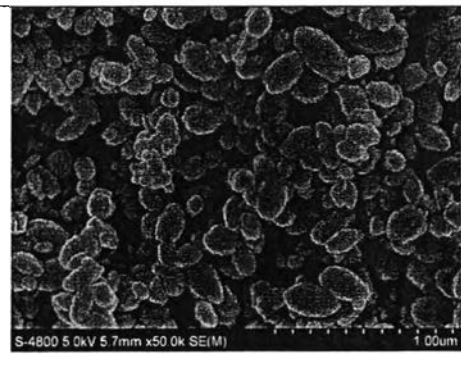	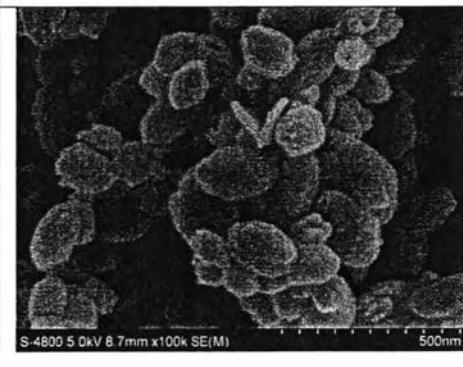

Note: Spherical-like particles were synthesized by the simple conditions, cubic-like particles were synthesized at very low amount of Fe(II), and ellipsoidal particles were synthesized by using NH_4OH instead of NaOH.

Table E2 Summary of FE-SEM images of the synthesized hematite nanoparticles under the effect of precursor concentrations

Precursor conc. (M)	FE-SEM images	
	Low magnification (50kX)	**High magnification (100kX)**
0.1	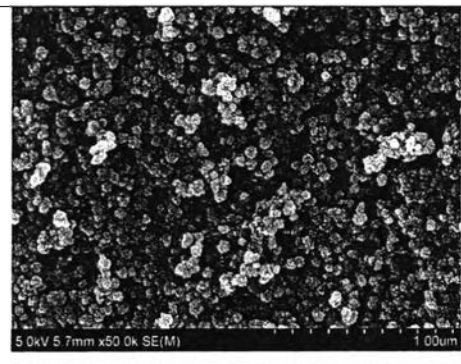	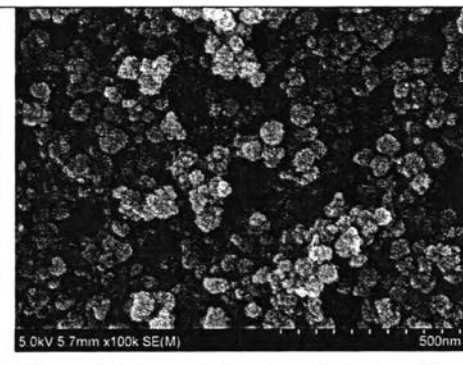
0.2	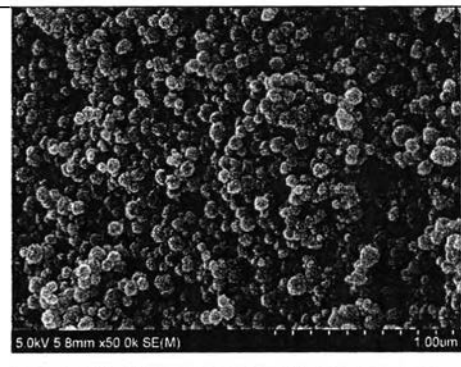	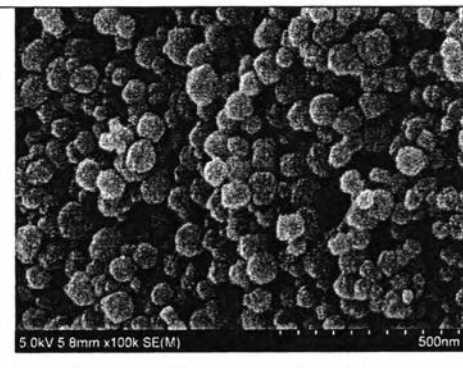
0.3	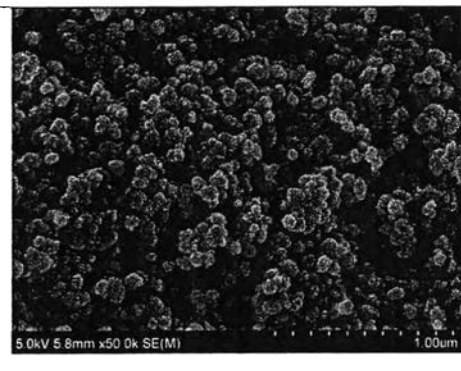	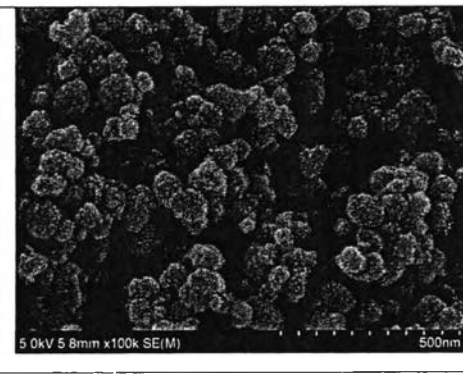

Precursor conc. (M)	FE-SEM images	
	Low magnification (50kX)	High magnification (100kX)
0.4	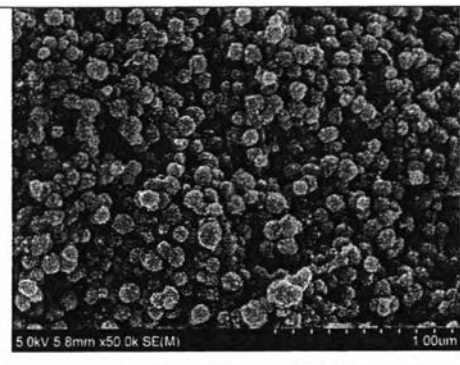	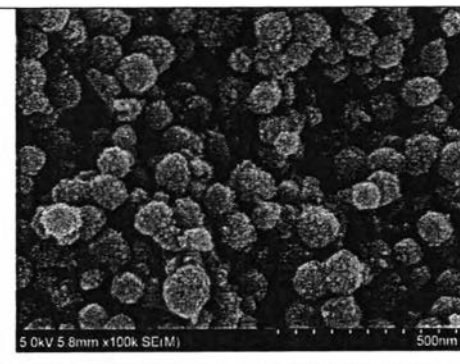
0.5	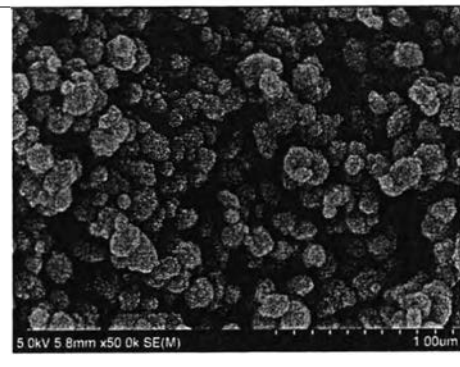	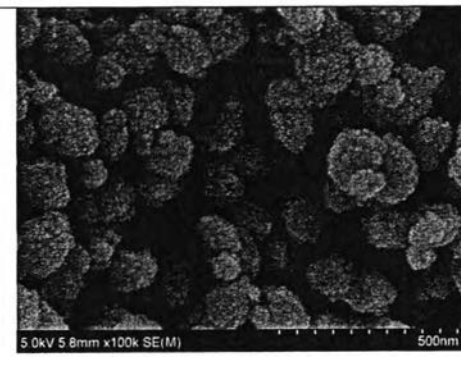

Table E3 Summary of FE-SEM images of the synthesized hematite nanoparticles under the effect of solution pHs

Solution pH	FE-SEM images	
	Low magnification (50kX)	**High magnification (100kX)**
pH 5	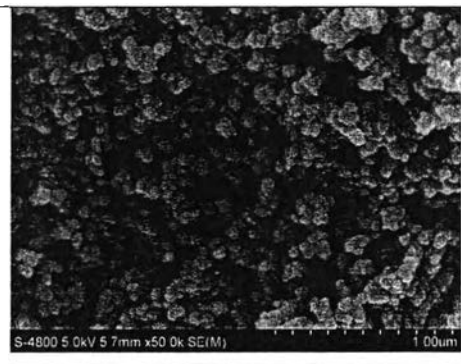	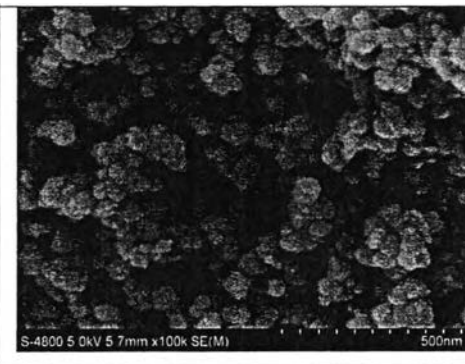
pH 6	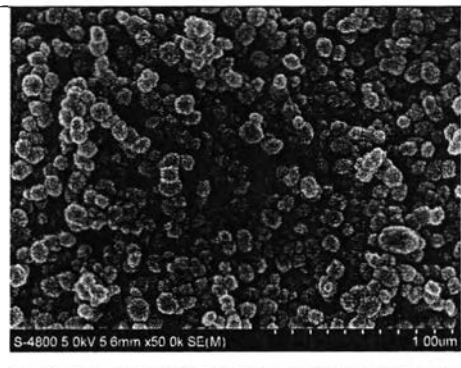	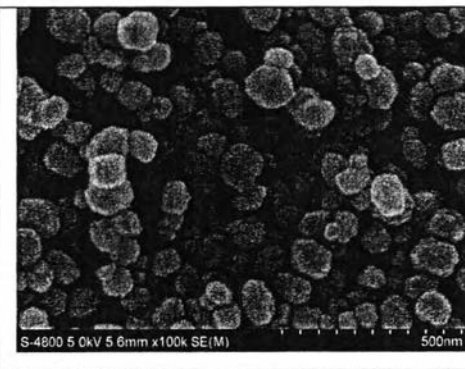
pH 7	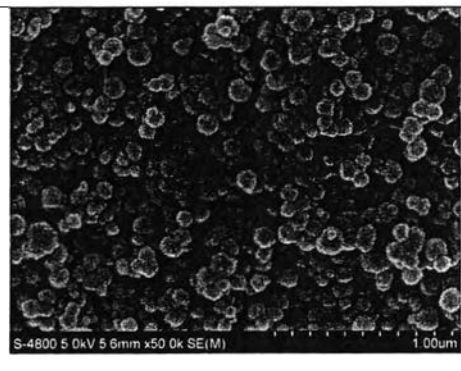	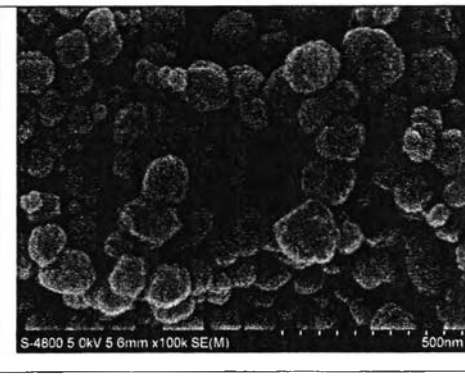

Solution pH	FE-SEM images	
	Low magnification (50kX)	High magnification (100kX)
pH 8	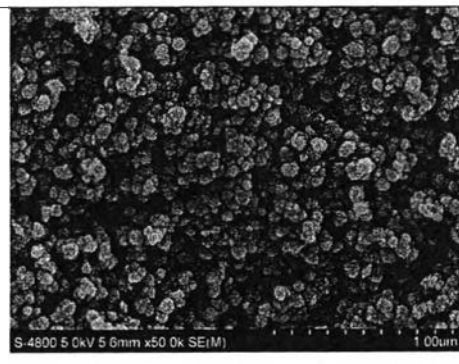	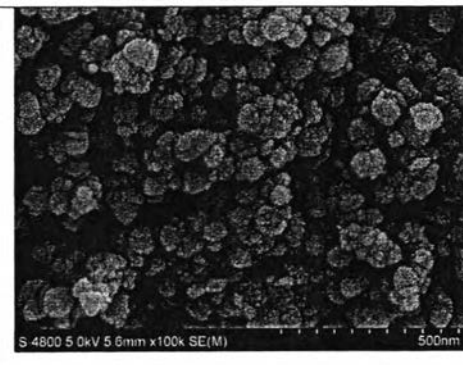
pH 9	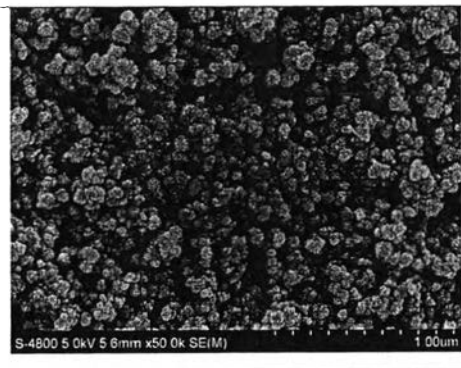	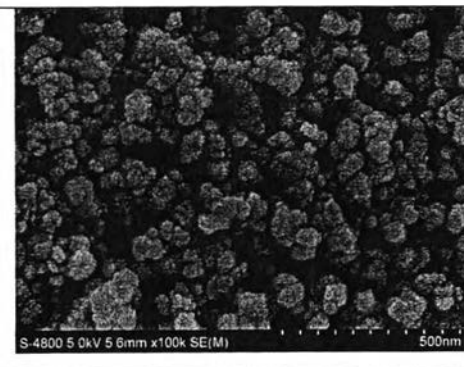

Table E4 Summary of FE-SEM images of the synthesized hematite nanoparticles under the effect of amounts of Fe(II)

$n_{Fe(II)}/n_{Fe(III)}$	FE-SEM images	
	Low magnification (50kX)	**High magnification (100kX)**
0.01	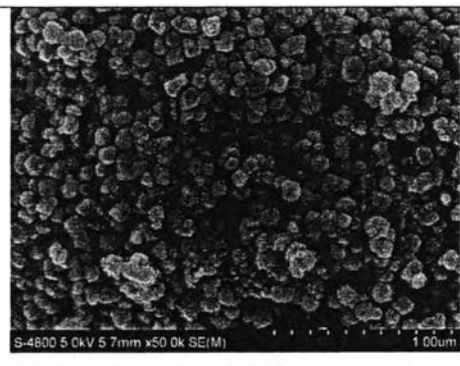	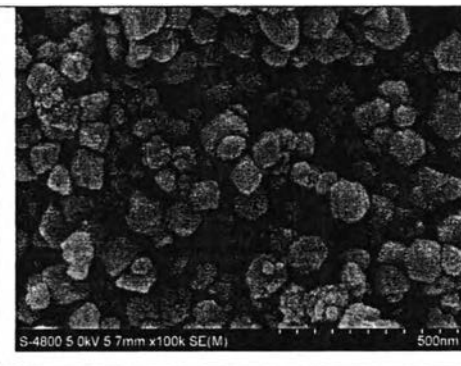
0.02	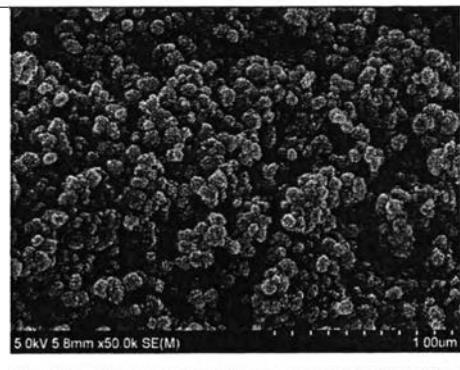	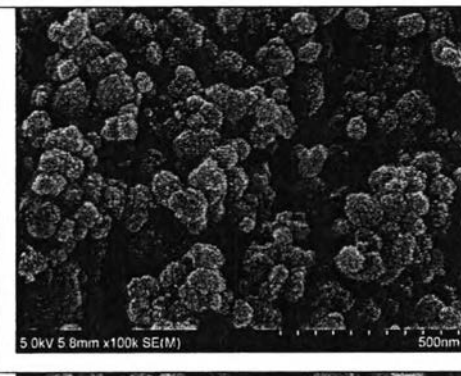
0.03	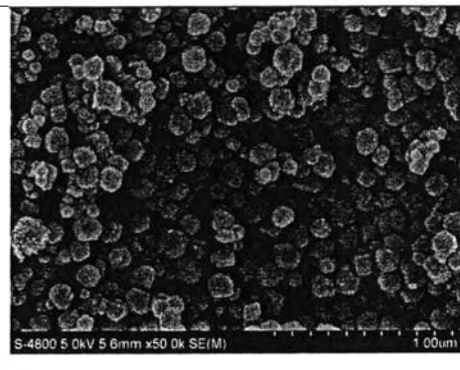	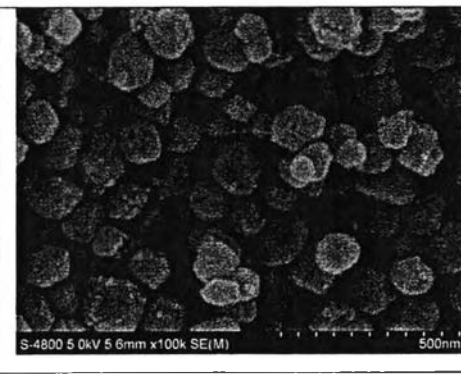

$n_{Fe(II)}/n_{Fe(III)}$	FE-SEM images	
	Low magnification (50kX)	High magnification (100kX)
0.04	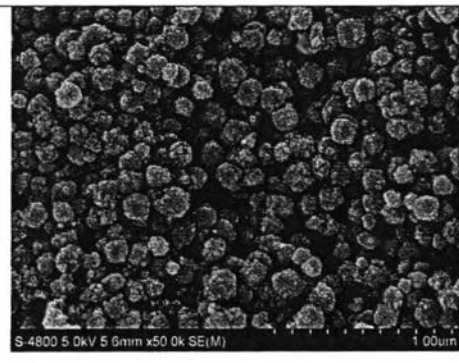	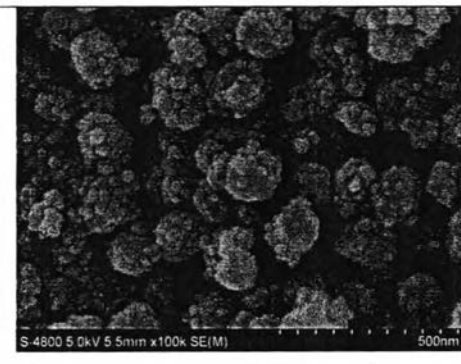
0.05	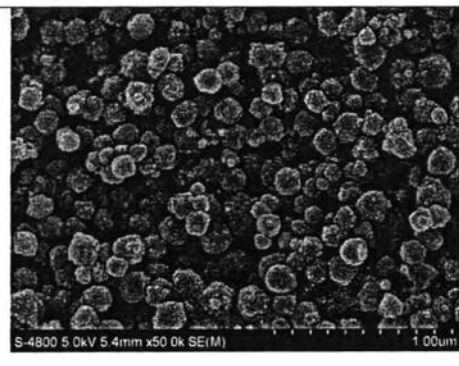	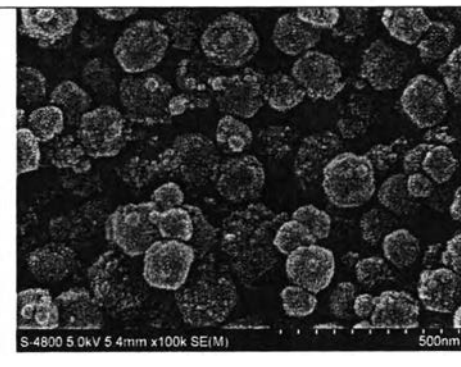

Table E5 Summary of FE-SEM images of the synthesized hematite nanoparticles under the effect of ionic strength (*I*) values

Ionic strength (*I*)	FE-SEM images	
	Low magnification (50kX)	High magnification (100kX)
1.0	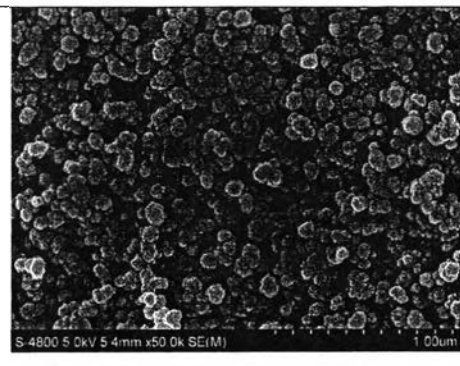	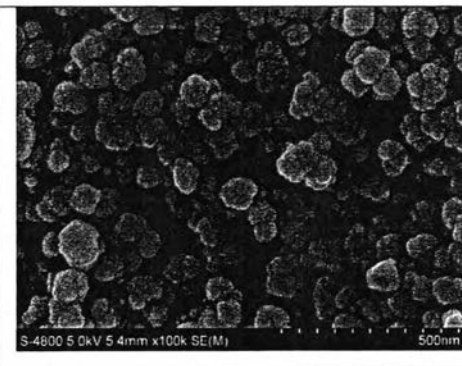
1.2	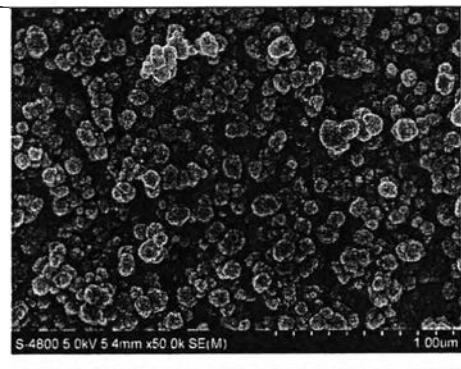	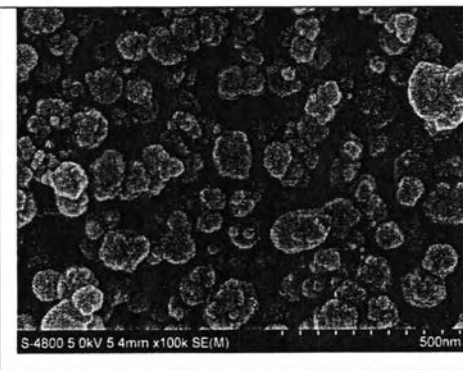
1.4	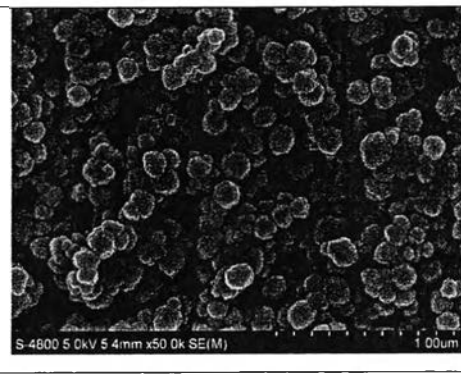	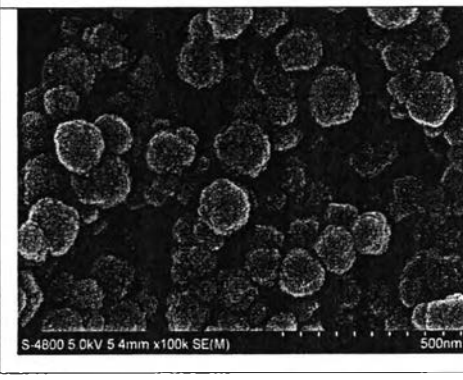

Ionic strength (*I*)	FE-SEM images	
	Low magnification (50kX)	High magnification (100kX)
1.6	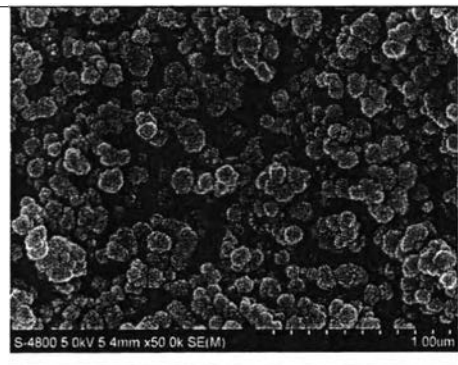	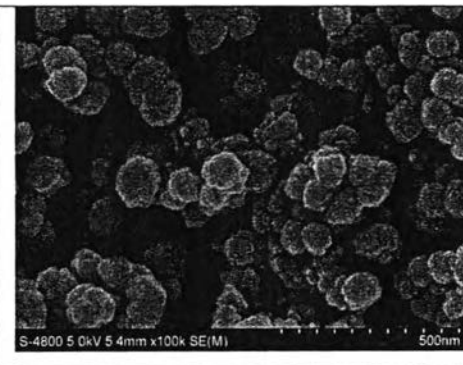
1.8	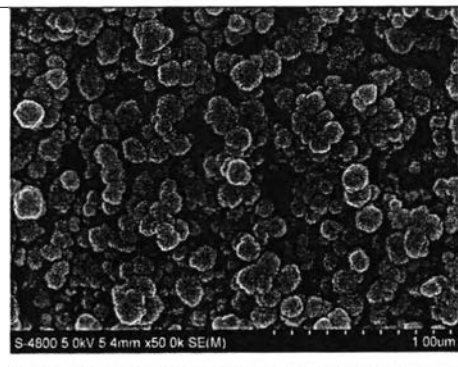	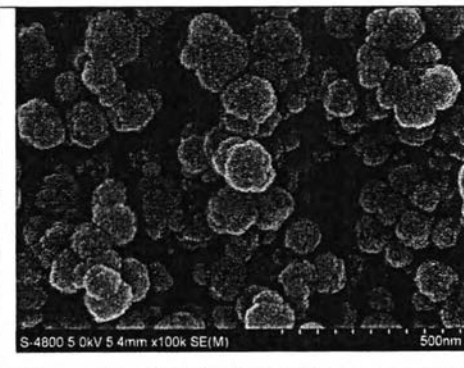
2.0	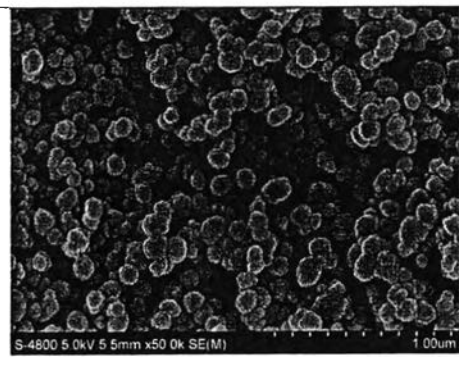	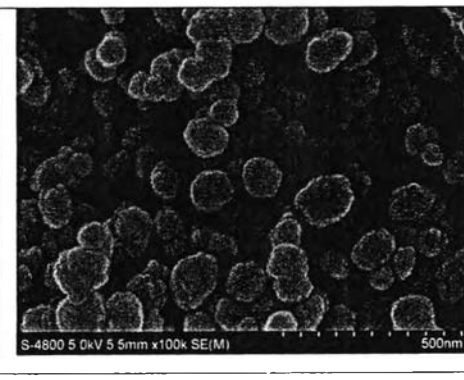

Table E6 Summary of FE-SEM images of the synthesized hematite nanoparticles under the effect of reaction temperatures

Reaction temp. (°C)	FE-SEM images	
	Low magnification (50kX)	**High magnification (100kX)**
60	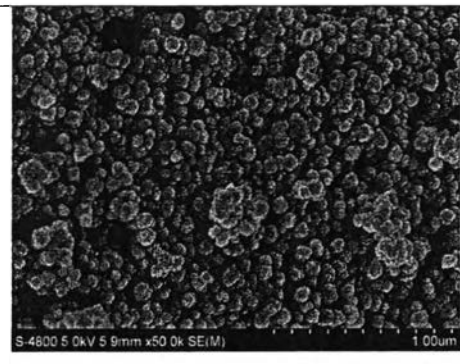	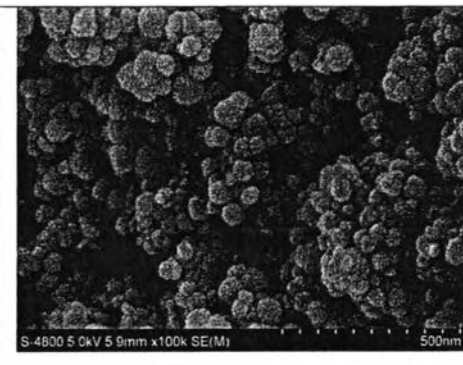
70	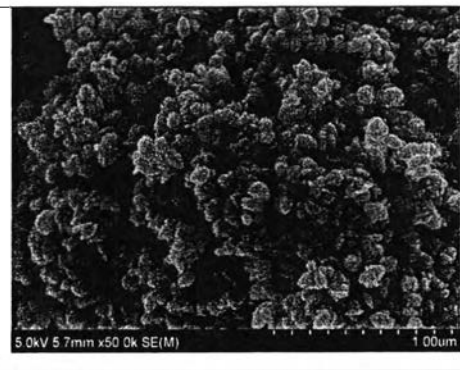	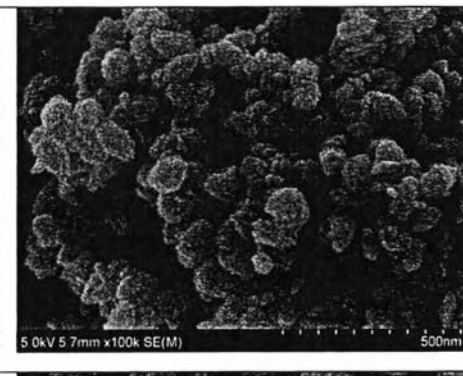
80	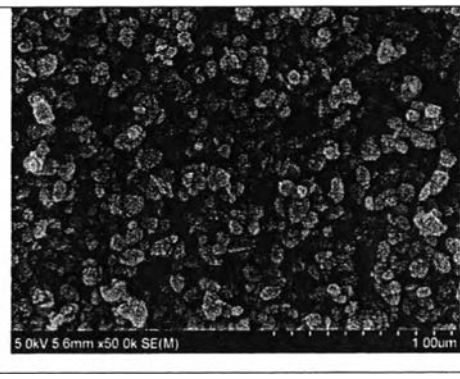	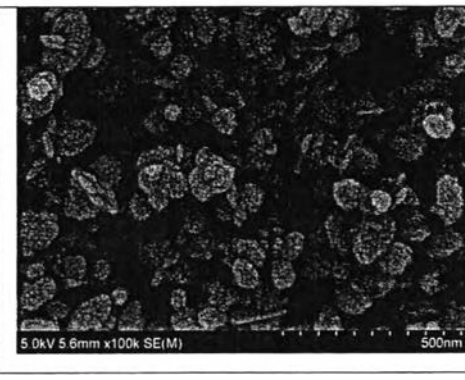

Reaction temp. (°C)	FE-SEM images	
	Low magnification (50kX)	High magnification (100kX)
90	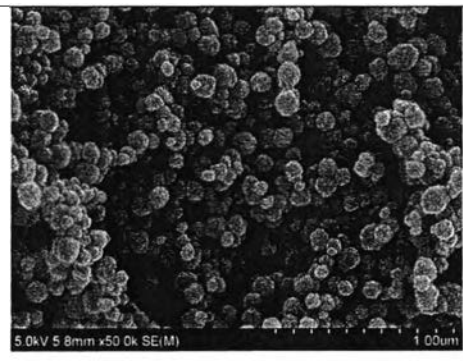	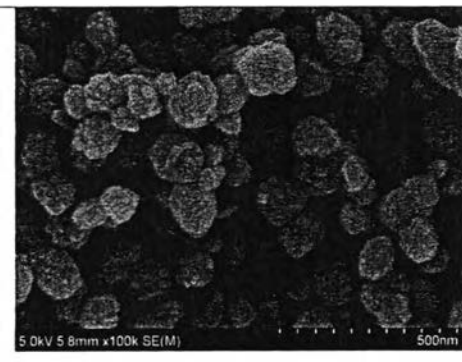
100	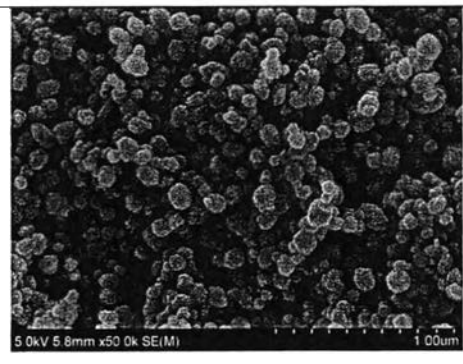	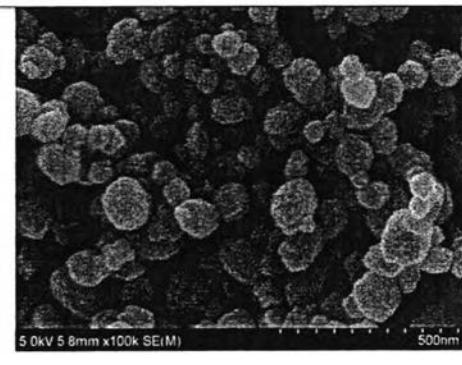

Table E7 Summary of FE-SEM images of the synthesized hematite nanoparticles under the effect of reaction times

Reaction time (min)	FE-SEM images	
	Low magnification (50kX)	**High magnification (100kX)**
10	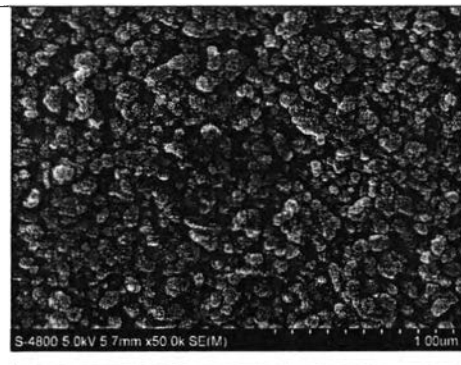	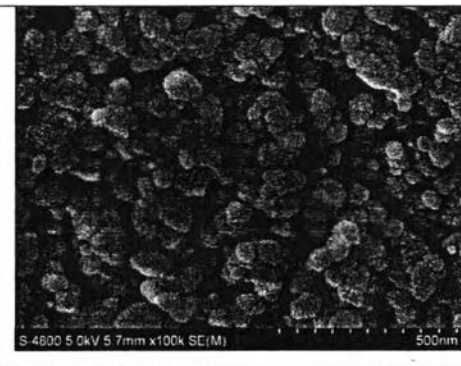
20	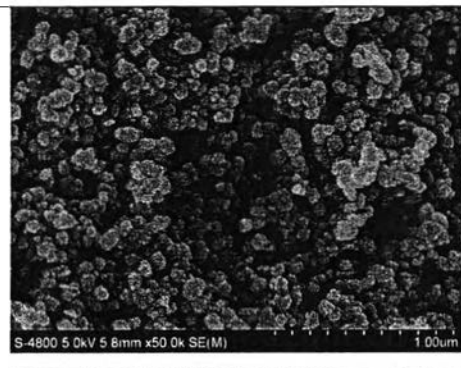	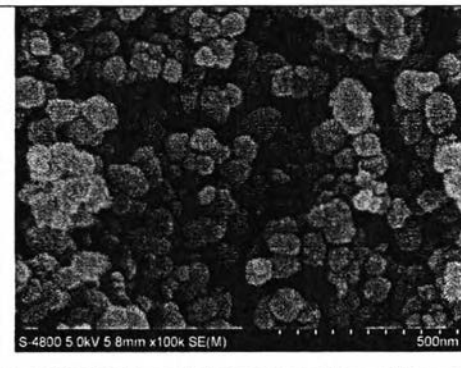
30	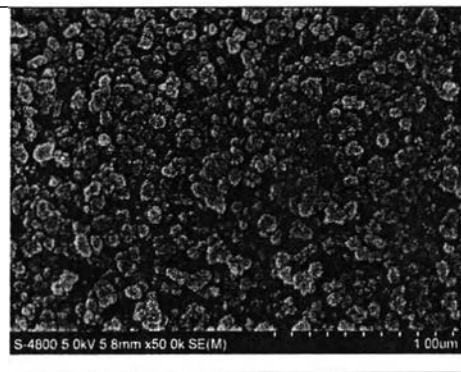	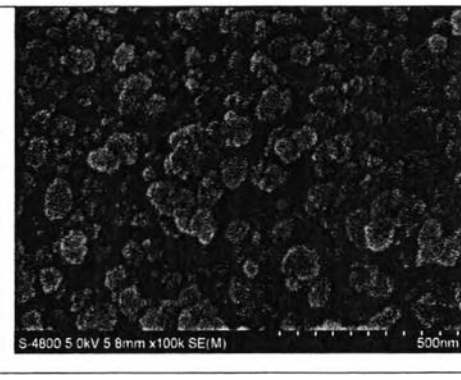

Reaction time (min)	FE-SEM images	
	Low magnification (50kX)	High magnification (100kX)
60	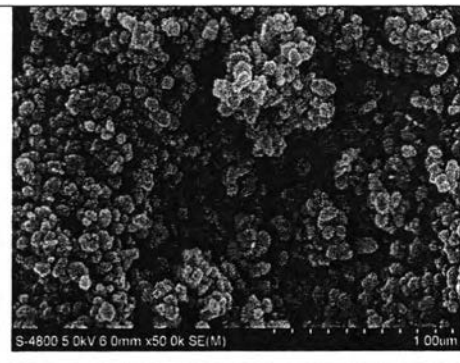	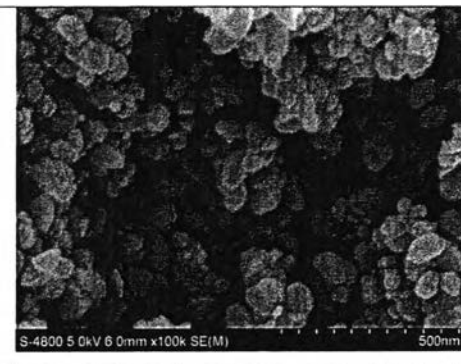
120	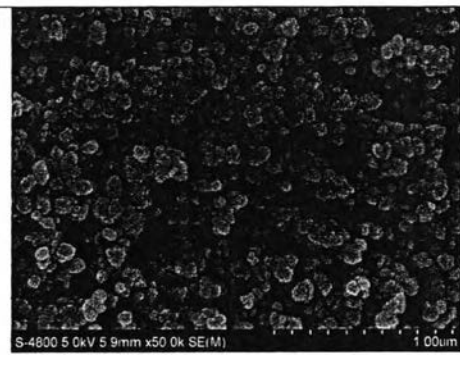	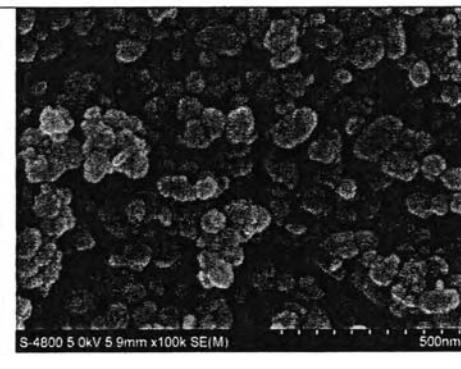

Appendix F Particle Sizes and Particle Size Distributions of the Synthesized Hematite Nanoparticles

The particle size and particle size distribution of the synthesized hematite particles were determined by the professional image processing and analysis software of SemAfore over 2-3 FE-SEM images by the quantitative statistical method. There are multiple definitions for mean diameter value because this value is associated with the basis of the distribution calculation (number, surface, volume). The general form of the mean particle diameter is defined using equation (F1) as follows:

$$D[p,q] = \left(\frac{\sum_{i=1}^{n} n_i D_i^p}{\sum_{i=1}^{n} n_i D_i^q}\right)^{\frac{1}{p-q}} \quad \text{(F1)}$$

where $D[p,q]$ = general form of the mean diameter
n_i = number of the i^{th} particle
D_i = diameter of i^{th} particle
$(p-q)$ = algebraic power of $D[p,q]$

The particle size of hematite could be characterized by $D[1,0]$ and $D[4,3]$ which are the number mean diameter (D_n; equation (F2)) and volume mean diameter (D_v; equation (F3)), respectively.

$$D_n = D[1,0] = \frac{\sum_{i=1}^{n} n_i D_i}{\sum_{i=1}^{n} n_i} \quad \text{(F2)}$$

$$D_v = D[4,3] = \frac{\sum_{i=1}^{n} n_1 D_i^4}{\sum_{i=1}^{n} n_i D_i^3} \quad \text{(F3)}$$

In addition, the particle size distribution index could be determined by the polydispersity index (PDI) using equation (F4) as follows:

$$PDI = \frac{D_v}{D_n} = \frac{D[4,3]}{D[1,0]} \quad \text{(F4)}$$

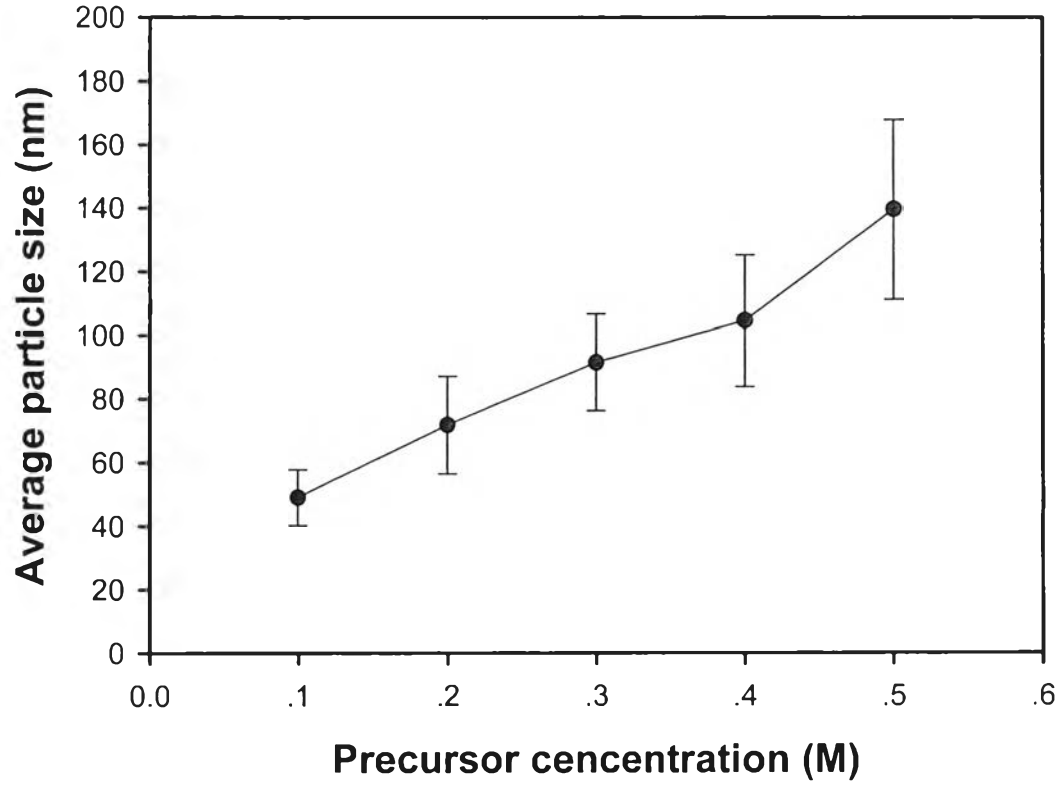

Figure F1 Average particle sizes of the synthesized hematite at various precursor concentrations with the constant $n_{Fe(II)}/n_{Fe(III)} = 0.02$, pH 7, 100 °C, and 1h.

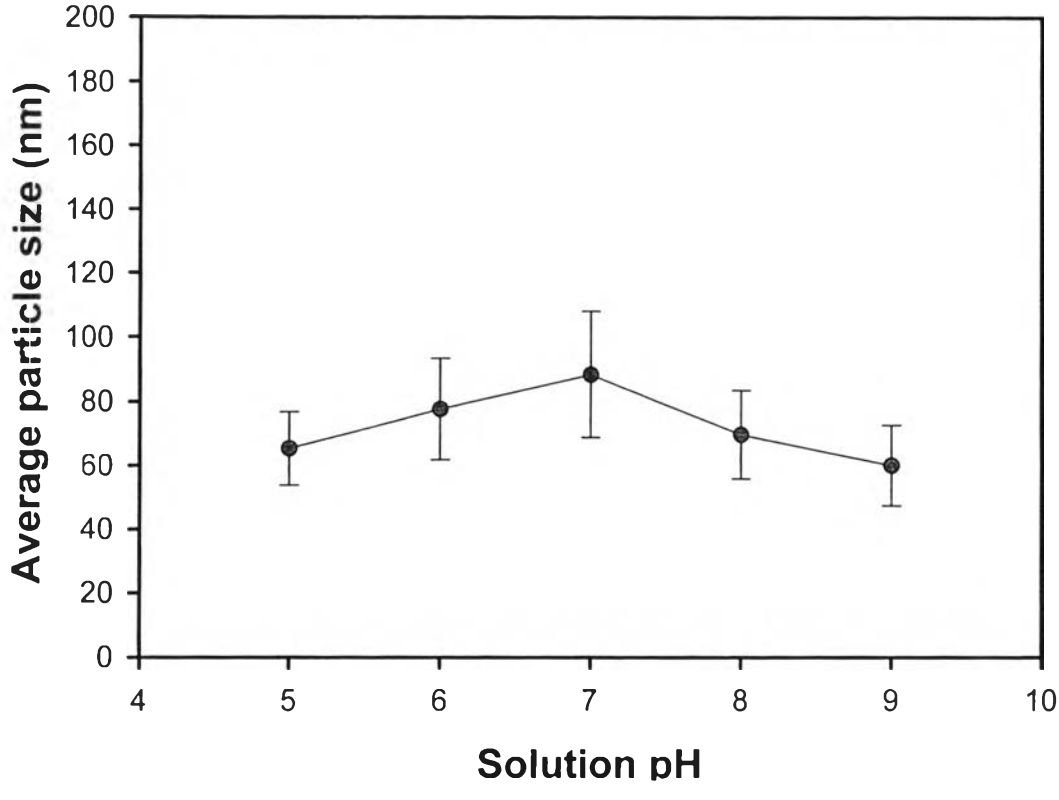

Figure F2 Average particle sizes of the synthesized hematite at various solution pHs with the constant C = 0.3 M, $n_{Fe(II)}/n_{Fe(III)}$ = 0.02, 100 °C, and 1h.

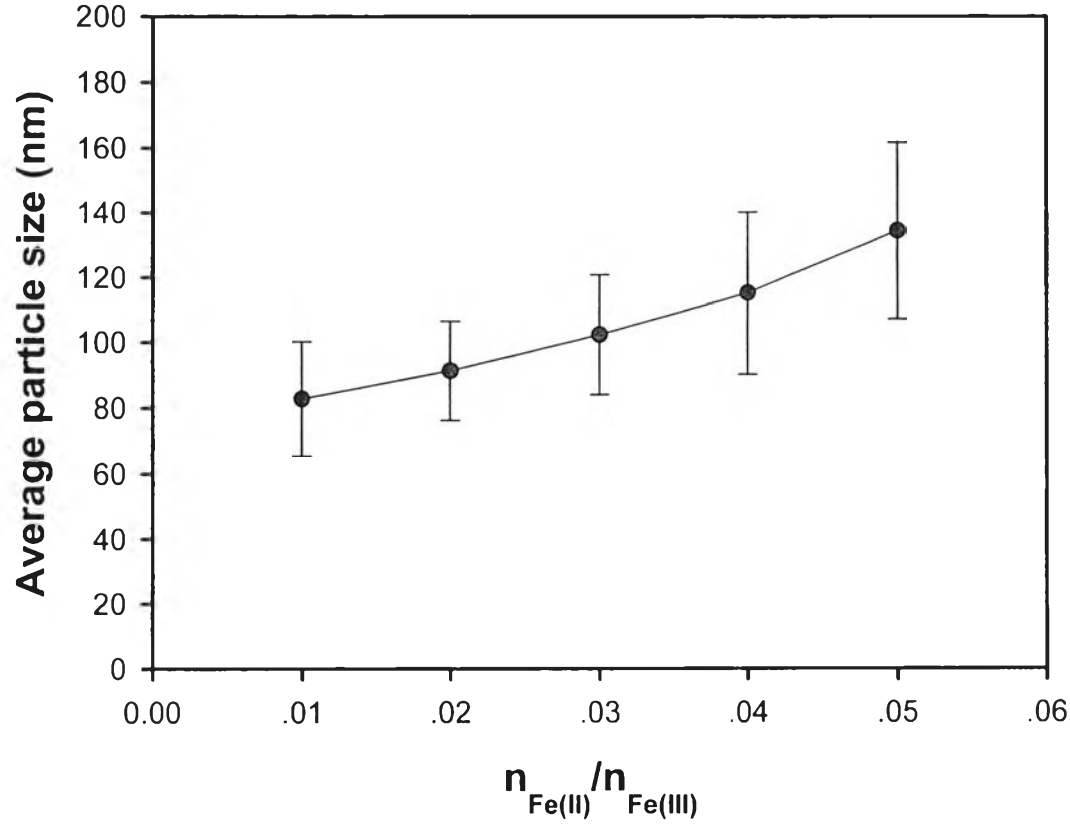

Figure F3 Average particle sizes of the synthesized hematite at various amounts of Fe(II) with the constant C = 0.3 M, pH 7, 100 °C, and 1h.

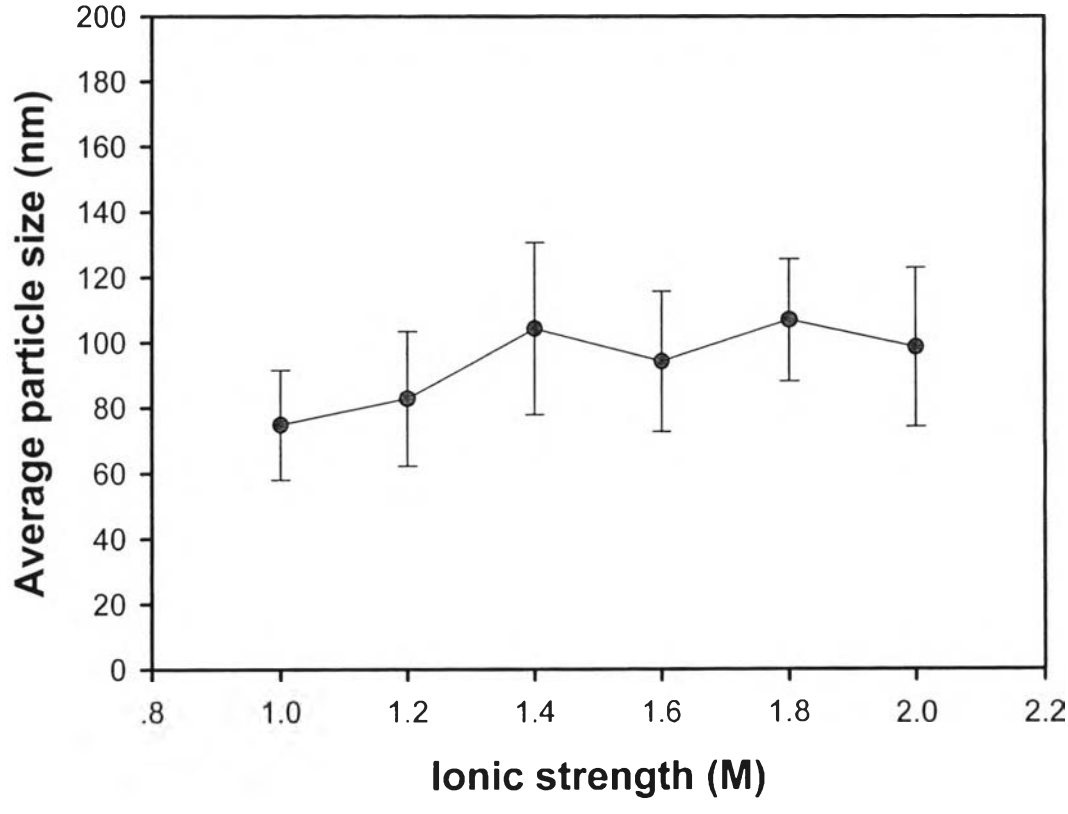

Figure F4 Average particle sizes of the synthesized hematite at various ionic strength (I) values with the constant C = 0.3 M, $n_{Fe(II)}/n_{Fe(III)}$ = 0.02, pH 7, 100 °C, and 1h.

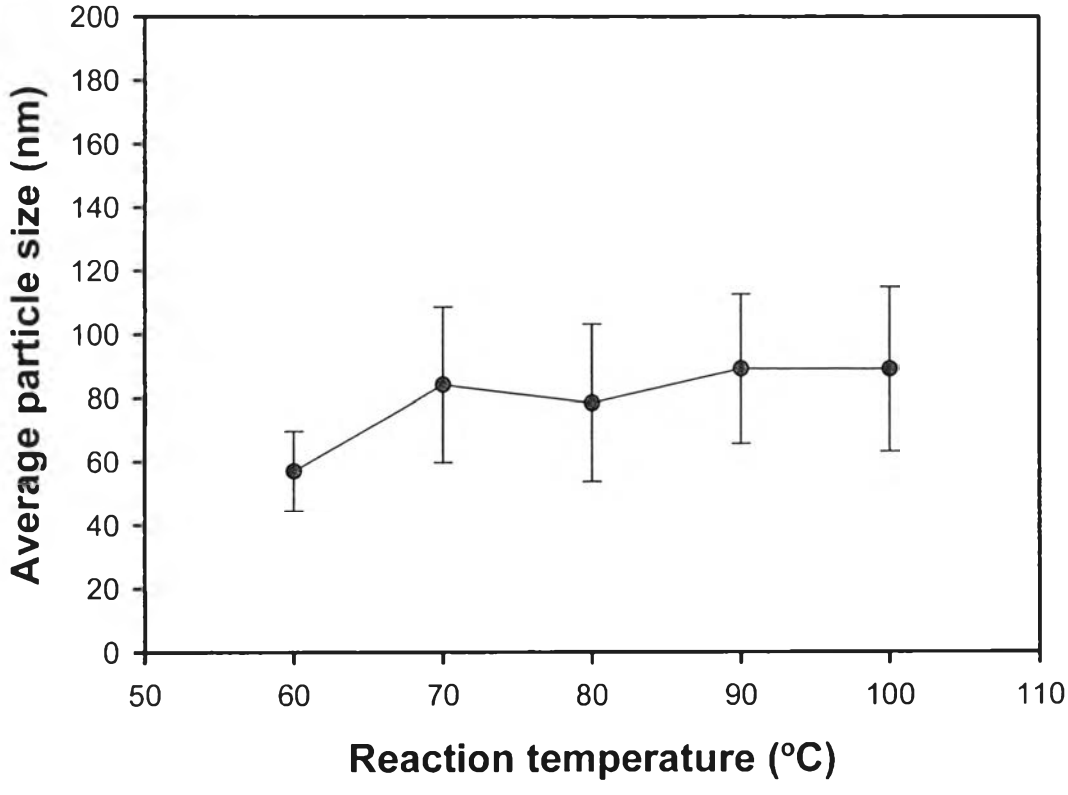

Figure F5 Average particle sizes of the synthesized hematite at reaction times with the constant $C = 0.3$ M, $n_{Fe(II)}/n_{Fe(III)} = 0.02$, pH 7, and 1h.

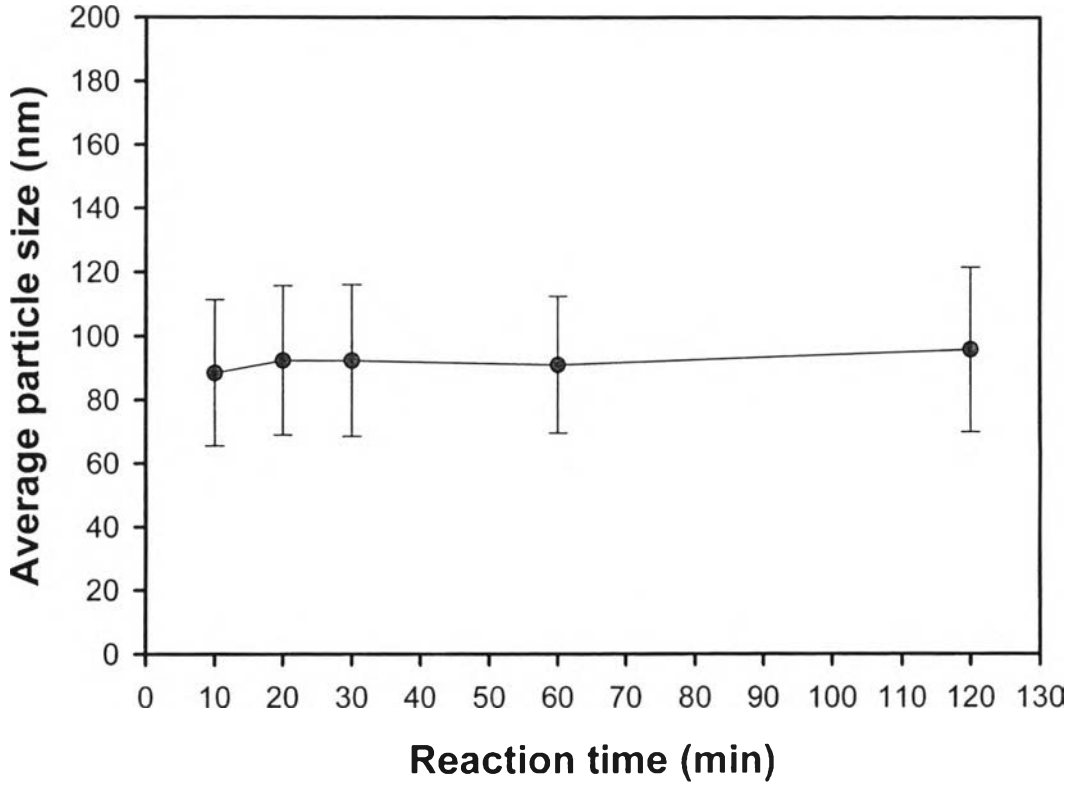

Figure F6 Average particle sizes of the synthesized hematite at reaction times with the constant C = 0.3 M, $n_{Fe(II)}/n_{Fe(III)}$ = 0.02, pH 7, and 100 °C.

Table F1 Summary of the average particle sizes and particle size distributions of the 2-line ferrihydrite precursor and the synthesized hematite nanoparticles with different morphologies

Sample	**Particle size (nm)** D_n ± **SD** D_v, **PDI**	**Particle size distribution**
Ferrihydrite	11.5 ± 2.0 12.5, 1.09	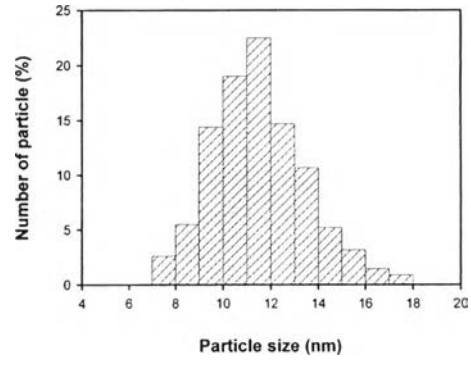
Spherical-like hematite	139.5 ± 28.2 153.3, 1.10	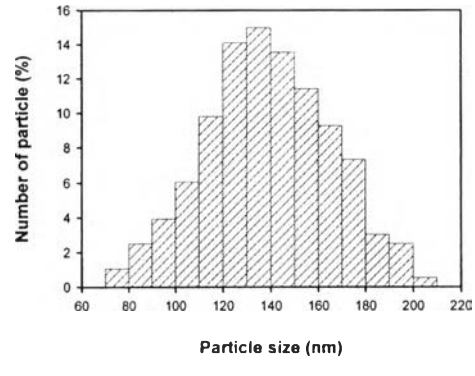

Sample	Particle size (nm) $D_n \pm$ SD D_v, PDI	Particle size distribution
Cubic-like hematite	127.5 ± 24.3 139.9, 1.10	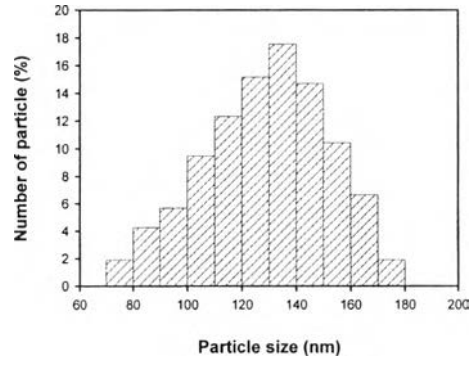
Ellipsoidal hematite	119.4 ± 44.3 167.3, 1.40	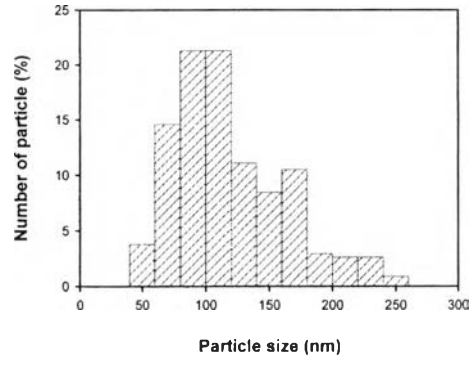

Note: Spherical-like particles were synthesized by the simple conditions, cubic-like particles were synthesized at very low amount of Fe(II), and ellipsoidal particles were synthesized by using NH_4OH instead of NaOH.

Table F2 Summary of the average particle sizes and particle size distributions of the synthesized hematite under the effect of precursor concentrations

Precursor conc. (M)	**Particle size (nm)** $D_n \pm$ SD D_v, PDI	**Particle size distribution**
0.1	49.3 ± 8.8 54.0, 1.10	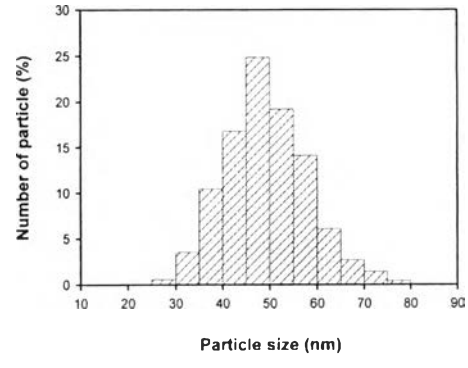
0.2	72.1 ± 15.3 81.6, 1.13	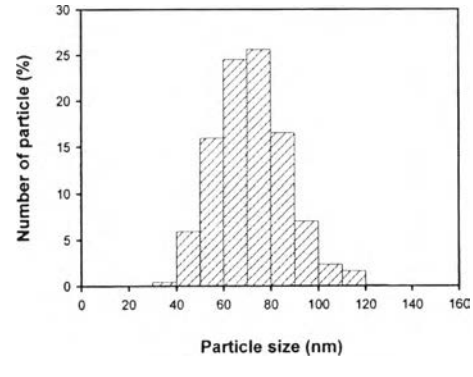

Precursor conc. (M)	**Particle size (nm)** D_n ± SD D_v, PDI	**Particle size distribution**
0.3	91.7 ± 15.1 99.4, 1.08	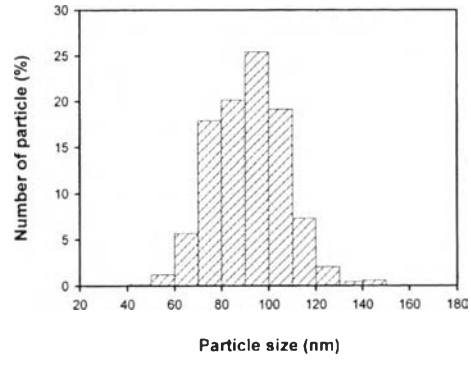
0.4	104.7 ± 20.6 111.8, 1.07	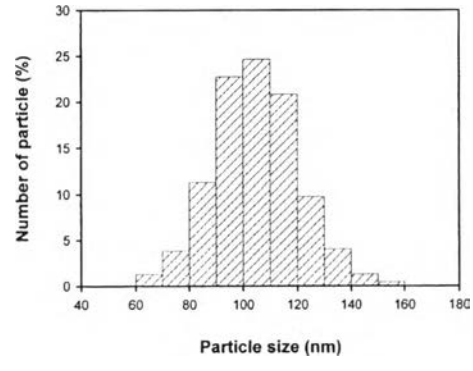
0.5	139.5 ± 28.2 153.3, 1.10	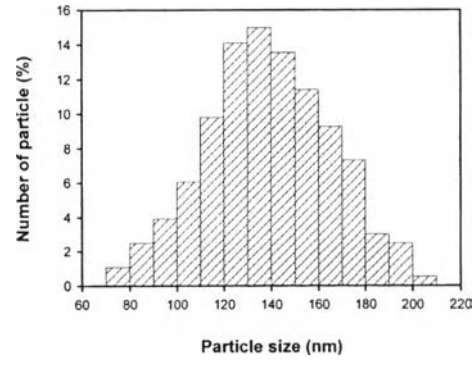

Table F3 Summary of the average particle sizes and particle size distributions of the synthesized hematite under the effect of solution pHs

Solution pH	**Particle size (nm)** D_n ± **SD** D_v, **PDI**	**Particle size distribution**
pH 5	65.3 ± 11.5 69.4, 1.06	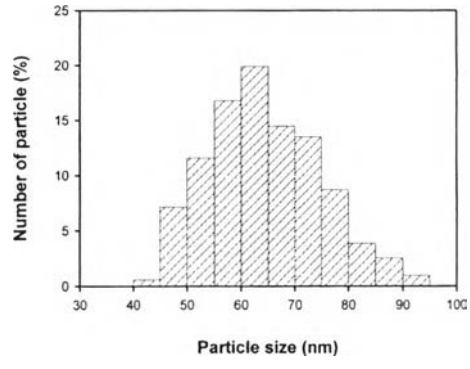
pH 6	77.7 ± 15.8 83.9, 1.08	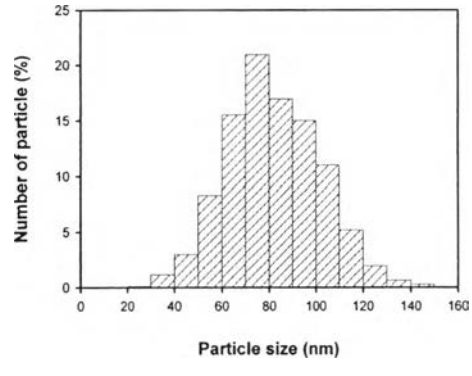
pH 7	88.4 ± 19.6 105.3, 1.19	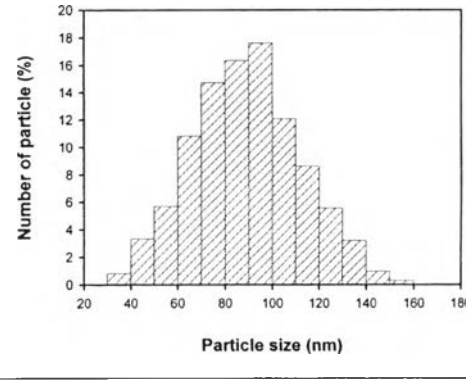

Solution pH	Particle size (nm) D_n ± SD D_v, PDI	Particle size distribution
pH 8	69.8 ± 13.8 76.1, 1.09	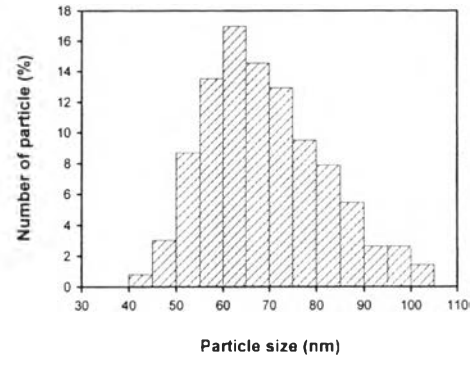
pH 9	60.1 ± 12.6 66.4, 1.10	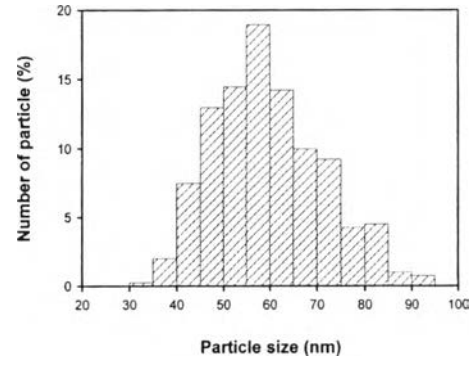

Table F4 Summary of the average particle sizes and particle size distributions of the synthesized hematite under the effect of amounts of Fe(II)

$n_{Fe(II)}/n_{Fe(III)}$	**Particle size (nm)** D_n ± SD D_v, PDI	**Particle size distribution**
0.01	83.1 ± 17.4 93.5, 1.13	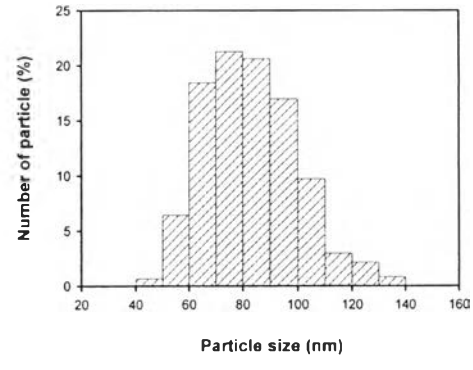
0.02	91.7 ± 15.1 99.4, 1.08	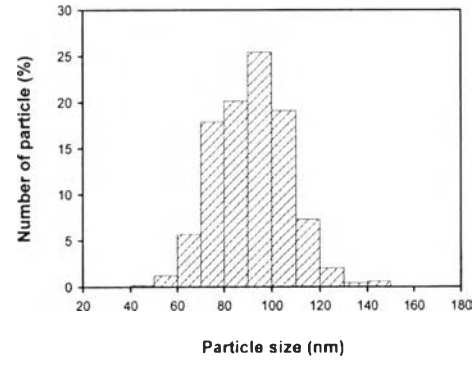
0.03	102.7 ± 18.3 115.1, 1.12	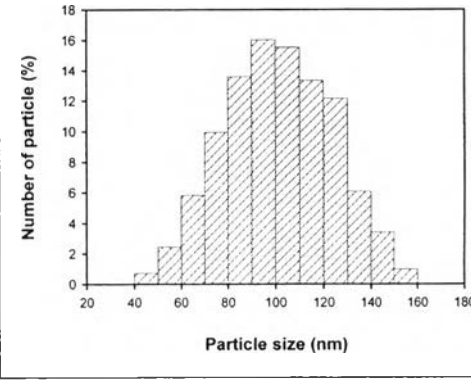

$n_{Fe(II)}/n_{Fe(III)}$	**Particle size (nm)** D_n ± SD D_v, PDI	**Particle size distribution**
0.04	115.4 ± 24.8 124.0, 1.07	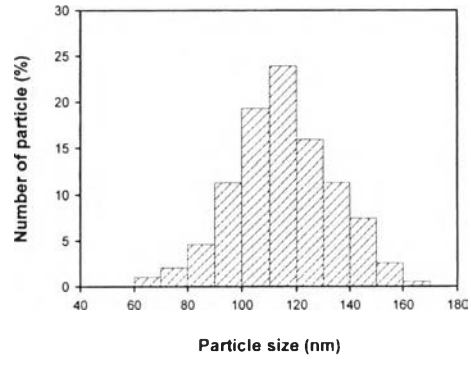
0.05	134.5 ± 27.2 147.1, 1.09	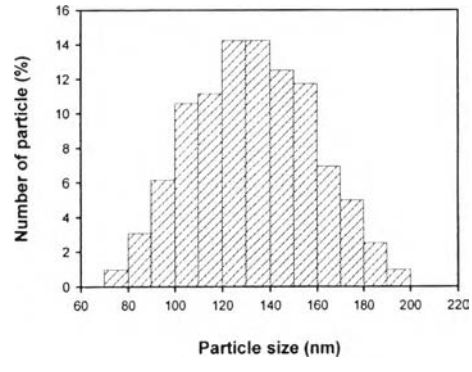

Table F5 Summary of the average particle sizes and particle size distributions of the synthesized hematite under the effect of ionic strength (I) values

Ionic strength (I)	**Particle size (nm)** **D_n ± SD** **D_v, PDI**	**Particle size distribution**
1.0	74.8 ± 16.8 85.7, 1.15	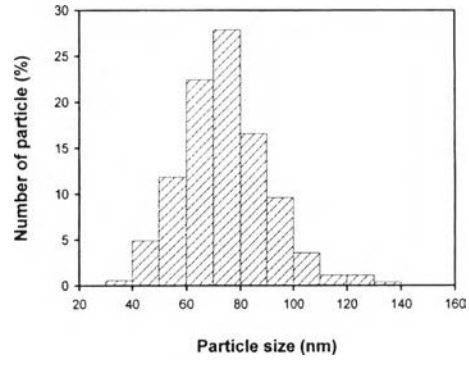
1.2	82.8 ± 20.6 95.0, 1.15	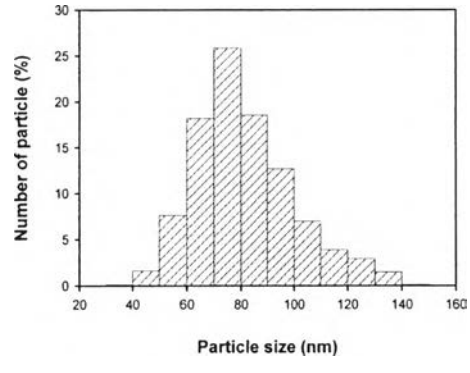
1.4	104.3 ± 26.4 121.3, 1.16	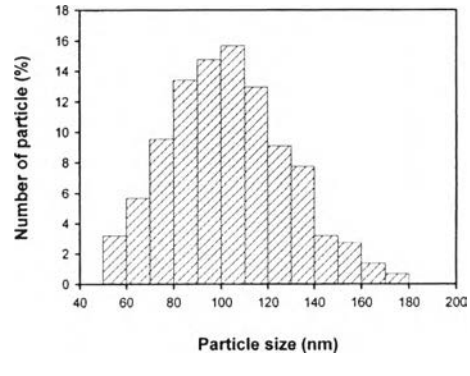

Ionic strength (*I*)	Particle size (nm) $D_n \pm$ SD D_v, PDI	Particle size distribution
1.6	94.2 ± 21.5 107.0, 1.14	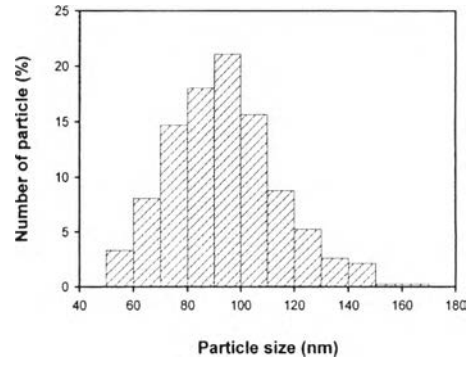
1.8	106.9 ± 18.7 116.7, 1.09	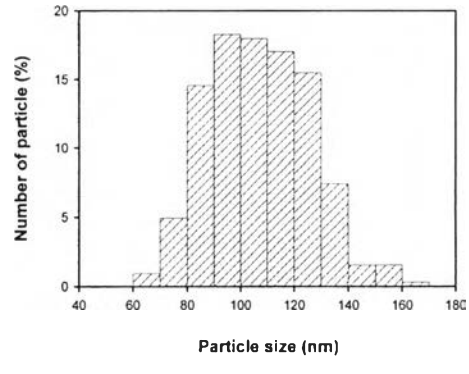
2.0	98.6 ± 24.4 109.8, 1.11	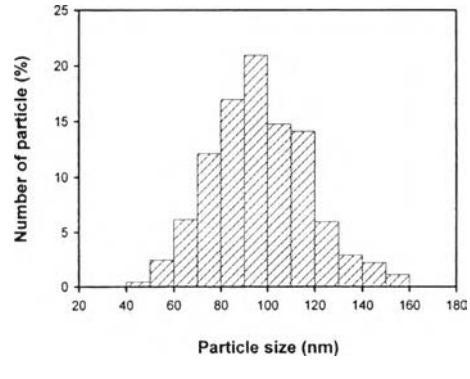

Table F6 Summary of the average particle sizes and particle size distributions of the synthesized hematite under the effect of reaction temperatures

Reaction temp. (°C)	**Particle size (nm)** $D_n \pm$ SD D_v, PDI	**Particle size distribution**
60	57.2 ± 12.6 63.3, 1.11	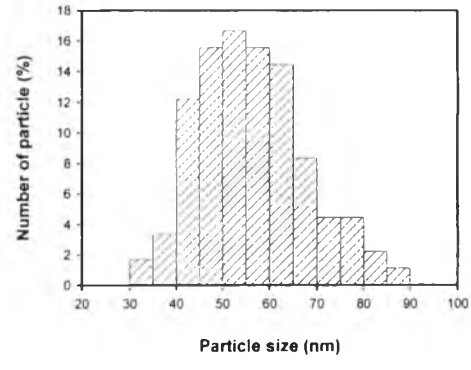
70	84.1 ± 24.2 98.9, 1.18	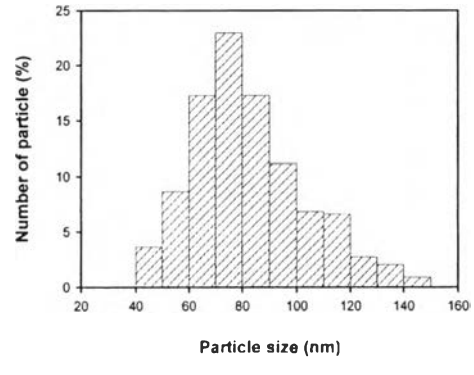
80	78.4 ± 24.6 96.7, 1.23	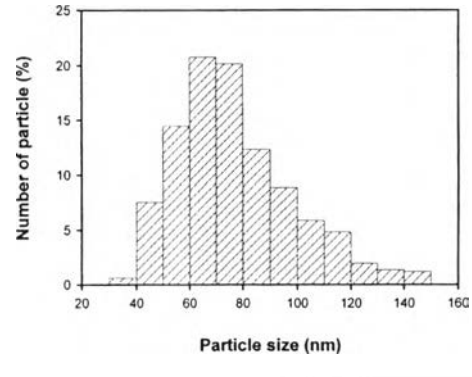

Reaction temp. (°C)	**Particle size (nm)** D_n ± **SD** D_v, **PDI**	**Particle size distribution**
90	89.1 ± 23.3 104.3, 1.17	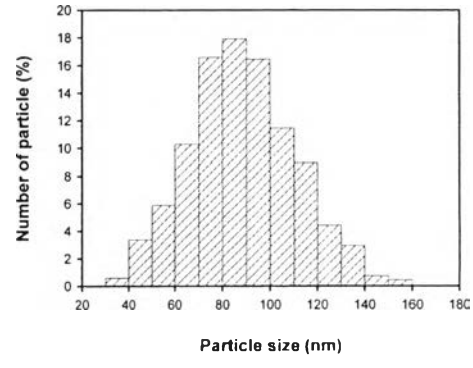
100	88.9 ± 25.7 106.1, 1.19	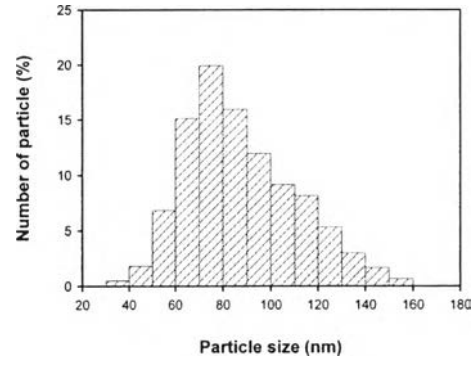

Table F7 Summary of the average particle sizes and particle size distributions of the synthesized hematite under the effect of reaction times

Reaction time (min)	**Particle size (nm)** $D_n \pm$ SD D_v, PDI	**Particle size distribution**
10	88.4 ± 22.9 102.1, 1.15	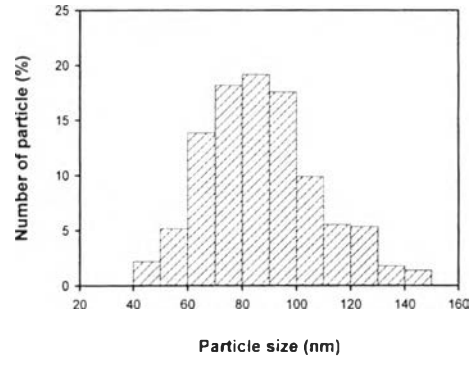
20	92.3 ± 23.4 104.0, 1.13	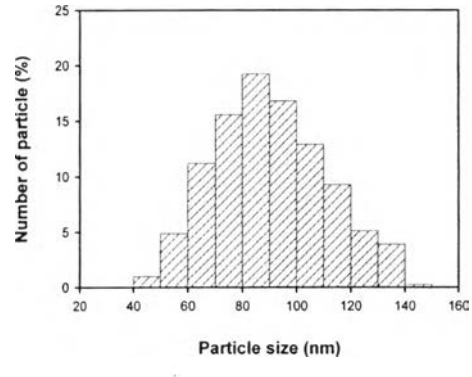
30	92.3 ± 23.8 106.2, 1.15	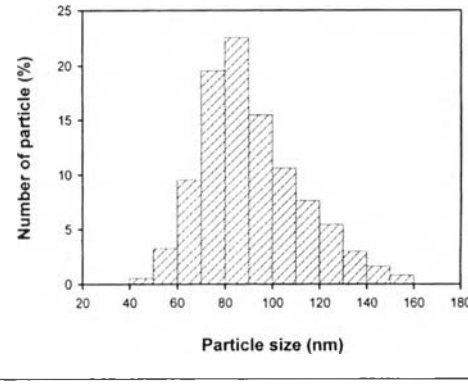

Reaction time (min)	**Particle size (nm)** $D_n \pm$ SD D_v, PDI	**Particle size distribution**
60	90.9 ± 21.4 103.6, 1.14	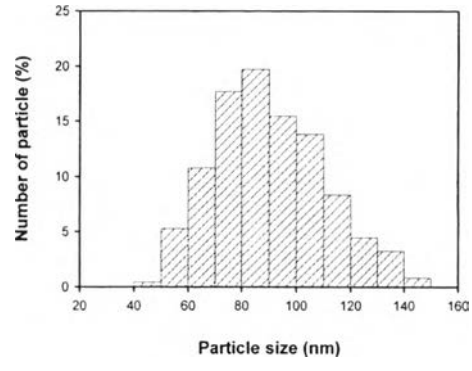
120	95.6± 25.8 110.0, 1.15	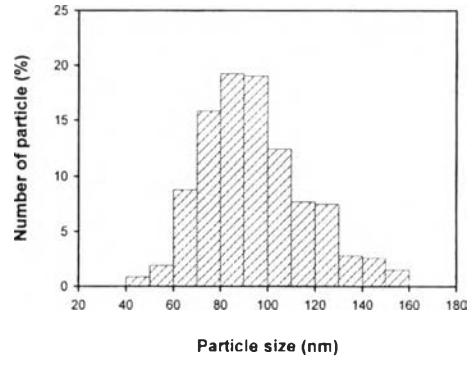

Appendix G Specific Surface Area Measurement of the Synthesized Hematite Nanoparticles

A surface area analyzer (Thermo finnigan, Sorptomatic 1990) was used to measure the specific surface area of the synthesized hematite particles. The absorbent sample was weighed and outgassed at 300 °C for 12 h under vacuum to eliminate volatile adsorbate on the surface. The data were obtained by adsorption and desorption with He and N_2 gases. The BET surface area was determined by using the static volumetric method.

In addition, the specific surface area (SSA) could be estimated from the particle size of the spherical particle using equation (G1) as follow:

$$SSA = \frac{6}{D[3,2] \times \rho_S} \tag{G1}$$

where SSA = specific surface area (m^2/g)

$D[3,2]$ = surface mean diameter (nm) or D_s

ρ_s = solid density (g/m^3) for hematite particle ρ_s is about 5.26×10^6 g/m^3

Note: This equation is strictly correct only for the spherical particles but may be used without correction for shape if the particles are not too asymmetrical and the surface mean diameter can be calculated from equation (G2) as follow:

$$D_S = D[3,2] = \frac{\sum_{i=1}^{n} n_1 D_i^3}{\sum_{i=1}^{n} n_i D_i^2} \tag{G2}$$

where n_i = number of the i^{th} particle

D_i = diameter of i^{th} particle

Table G1 Summary of the specific surface area of the synthesized hematite nano-particles with different particle sizes and morphologies

Sample		Specific surface area (m^2/g)	
Particle shape	**Particle size (*D[3,2]*; nm)**	**Calculated**	**BET**
Sphere	52.4	21.7	55.4
Sphere	96.8	11.8	29.4
Sphere	148.9	7.7	18.5
Cube	136.7	8.3	13.7
Ellipsoid	151.7	7.5	7.6

Appendix H Electrical Conductivity Measurement of the Synthesized Hematite Nanoparticles

An electrometer (Keithley, 6517A), with a custom-built two-point probe, was used to measure the electrical conductivity which is the inversion of specific resistivity (ρ) that indicates the ability of material to transport electrical charge. The meter consisted of a probe making contact on the surface of the sample in a disc shape. This probe was connected to a power supplier source for a constant source and for reading current. The applied voltage was plotted versus the resultant current to determine the linear Ohmic regime of each sample based on the Van der Pauw method. The applied voltage and the current in the linear Ohmic regime were converted to the electrical conductivity of the sample using equation (H1) as follow:

$$\sigma = \frac{1}{\rho} = \frac{1}{R_S \times t} = \frac{I}{K \times V \times t} = \frac{slope}{K \times t} \qquad \text{(H1)}$$

where σ is the specific conductivity (S/cm), ρ is the specific resistivity (Ω.cm), R_s is the sheet resistivity (Ω), I is the resultant current (A), K is the geometric correction factor, V is the applied voltage (V), and t is the thickness of the disc sample (cm).

The geometrical correction factor was taken into account of geometric effects, depending on the configuration and probe tip spacing and was determined by using standard materials where specific resistivity values were known; we used silicon wafer chips (SiO_2). In our case, the sheet resistivity was measured by using the two-point probe and then the geometric correction factor was calculated by equation (H2) as follow:

$$K = \frac{\rho}{R \times t} = \frac{I \times \rho}{V \times t} = slope \times R_S \qquad \text{(H2)}$$

where K is the geometric correction factor, ρ is the known resistivity of standard silicon wafer (Ω.cm), t is the film thickness (cm), R is the film resistance (Ω), and I is the resultant current (A).

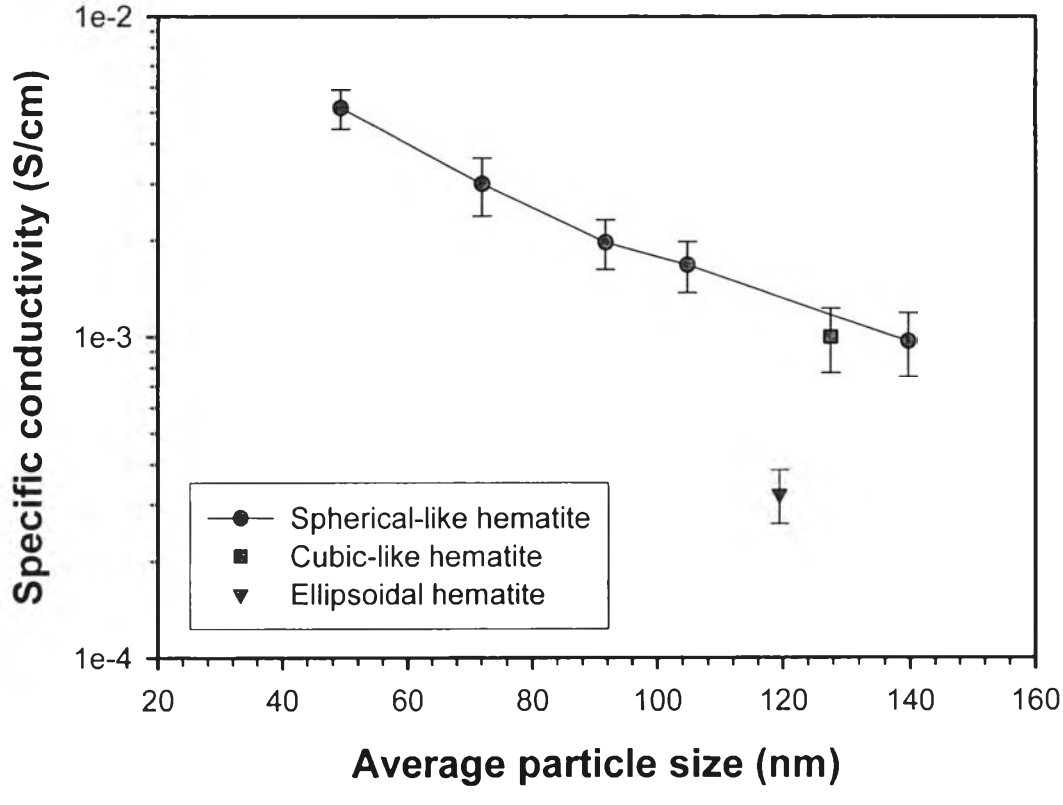

Figure H1 Specific conductivities of the synthesized hematite nanoparticles with different particle sizes.

Table H1 Summary of the specific conductivities of the 2-line ferrihydrite precursor and the synthesized hematite nanoparticles with different particle sizes and morphologies

Sample	Particle size (nm) ($\bar{X}$ ± SD)	Specific conductivity (S/cm)	
		Avg.	SD
Ferrihydrite	11.5 ± 2.0	5.51E-02	8.47E-03
Hematite *C* = 0.1 M	49.3 ± 8.8	5.16E-03	7.20E-04
Hematite *C* = 0.2 M	72.1 ± 15.3	2.99E-03	6.13E-04
Hematite *C* = 0.3 M	91.7 ± 15.1	1.97E-03	3.46E-04
Hematite *C* = 0.4 M	104.7 ± 20.6	1.68E-03	3.03E-04
Hematite *C* = 0.5 M	139.5 ± 28.2	9.72E-04	2.20E-04
Cubic-like hematite	127.5 ± 24.3	1.00E-03	2.29E-04
Ellipsoidal hematite	119.4 ± 44.3	3.22E-04	6.13E-05

Note: The synthesized hematite particles using precursor concentration 0.1-0.5 M possessed the spherical-like morphology.

Table H2 Raw data for determination of the linear Ohmic regime to calibrate probe by using a standard silicon wafer (R_s = 107.373 Ω)

Applied voltage (V)	Current (μA)				Slope	K
	#1	#2	#3	Avg.		
0.150	1.11237	1.10720	1.10092	**1.10683**		
0.140	1.00173	1.03114	1.04587	**1.02625**		
0.130	0.95143	0.95578	0.93653	**0.94791**		
0.120	0.87137	0.86263	0.86033	**0.86478**		
0.110	0.79486	0.78845	0.81494	**0.79942**		
0.100	0.71164	0.71788	0.70909	**0.71287**		
0.090	0.68512	0.69277	0.64487	**0.67425**		
0.080	0.65394	0.63814	0.63196	**0.64135**	**6.8574E-06**	**7.3630E-04**
0.070	0.56354	0.56817	0.55963	**0.56378**		
0.060	0.49270	0.48635	0.48984	**0.48963**		
0.050	0.41209	0.39410	0.38765	**0.39795**		
0.040	0.33994	0.33598	0.34286	**0.33960**		
0.030	0.26485	0.26491	0.26216	**0.26397**		
0.020	0.18628	0.18342	0.18279	**0.18416**		
0.010	0.12530	0.12617	0.12626	**0.12591**		

Example H1: Calculation of the geometric correction factor (K)

The geometric correction factor was calculated by equation (G2) as follow:

$$K = slope \times R_s$$

$$K = (6.8574 \times 10^{-6}\Omega^{-1})(107.373\ \Omega)$$

$$K = 7.3630 \times 10^{-4}$$

So, the geometric correction factor (K) was 7.3630 x 10^{-4}.

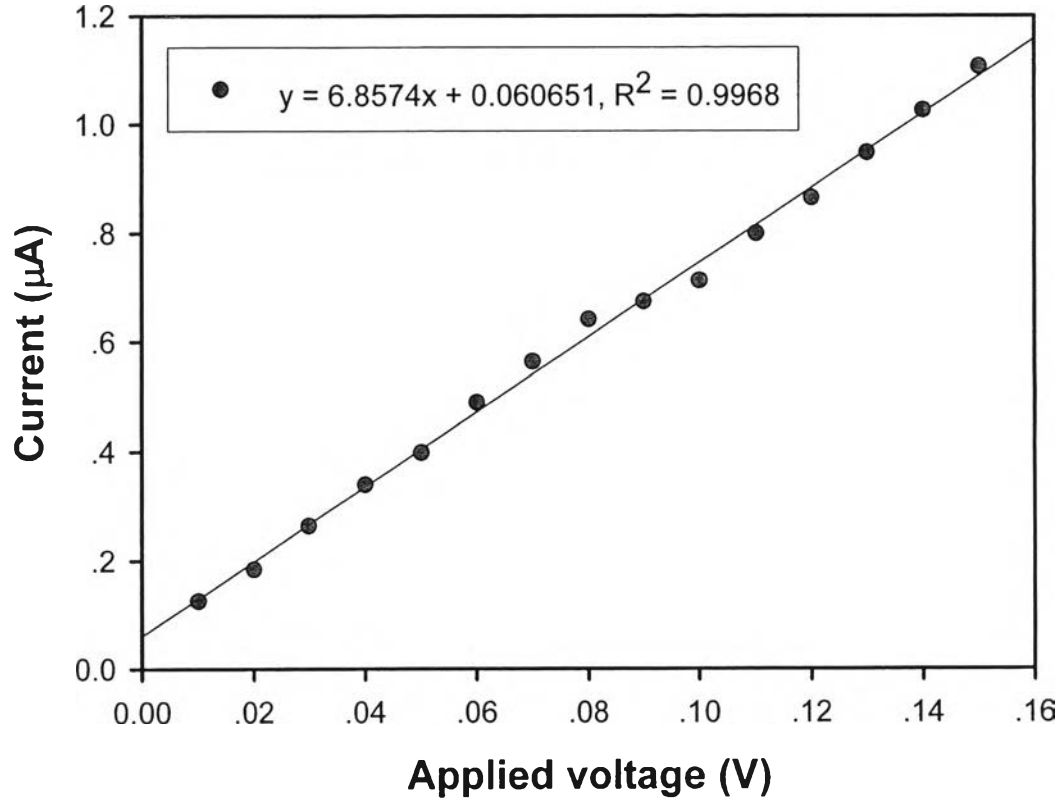

Figure H2 The linear Ohmic regime plot of the standard silicon wafer (R_s = 107.373 Ω).

Table H3 Raw data for determination of the linear Ohmic regime and the specific conductivities of the 2-line ferrihydrite precursor

Sample	Thickness (cm)	Applied voltage (V)	Current (nA)				Specific conductivity (S/cm)
			#1	#2	#3	Avg.	
No.1	0.0425	0.120	260.366	258.398	256.157	**258.307**	6.41E-02
	0.0443	0.110	238.771	239.076	238.794	**238.880**	
	0.0429	0.100	212.544	208.989	209.603	**210.379**	
	0.0462	0.090	190.718	189.325	190.273	**190.105**	
	0.0420	0.080	169.817	170.431	171.017	**170.422**	
	0.0454	0.070	150.569	150.669	149.764	**150.334**	
	0.0439	0.060	131.997	131.006	131.417	**131.474**	
		0.050	109.439	108.197	107.248	**108.295**	
		0.040	89.042	90.235	90.438	**89.905**	
		0.030	74.026	73.488	70.755	**72.756**	
No.2	0.0449	0.120	231.494	230.336	232.883	**231.571**	5.38E-02
	0.0485	0.110	209.629	211.319	213.010	**211.319**	
	0.0433	0.100	204.499	203.482	201.651	**203.211**	
	0.0478	0.090	181.660	184.221	182.940	**182.940**	
	0.0428	0.080	160.010	161.138	162.589	**161.246**	
	0.0437	0.070	147.291	145.965	148.469	**147.242**	
	0.0452	0.060	129.172	129.821	130.600	**129.864**	
		0.050	106.473	105.523	104.785	**105.594**	
		0.040	87.890	88.863	88.421	**88.391**	
		0.030	72.370	71.791	72.877	**72.346**	
No.3	0.0493	0.120	203.631	205.480	207.124	**205.412**	4.73E-02
	0.0475	0.110	179.992	182.167	181.261	**181.140**	
	0.0451	0.100	174.564	173.523	172.482	**173.523**	
	0.0494	0.090	155.285	157.946	156.537	**156.590**	
	0.0495	0.080	132.777	132.113	133.707	**132.866**	
	0.0476	0.070	122.104	121.376	120.405	**121.295**	
	0.0481	0.060	102.909	103.530	104.462	**103.634**	
		0.050	82.683	83.851	83.434	**83.322**	
		0.040	71.609	71.107	72.182	**71.633**	
		0.030	52.239	52.502	52.869	**52.537**	
Average specific conductivity							**5.51E-02**
Standard deviation							**8.47E-03**

Note: The bold values are the average values of the data.

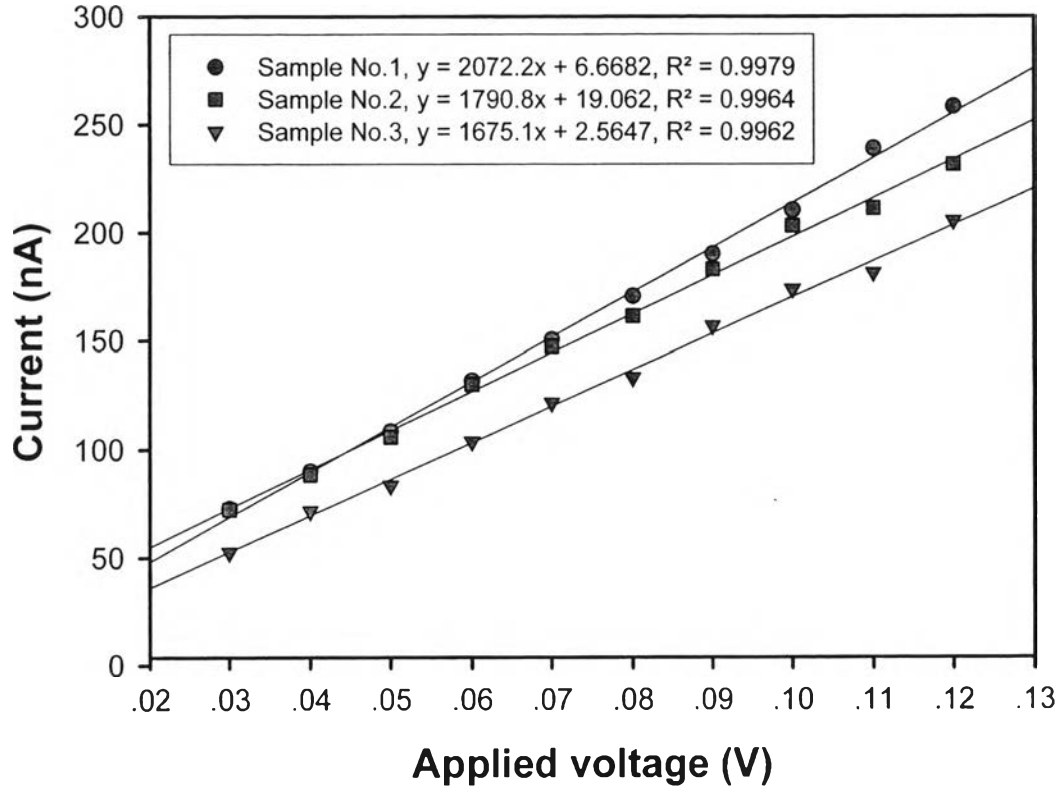

Figure H3 The linear Ohmic regime plots of the 2-line ferrihydrite precursor.

Example H2: Calculation of the specific conductivity (σ) of the sample no.1

The specific conductivity (σ) was calculated by equation (G2) as follow:

$$\sigma = \frac{slope}{K \times t}$$

$$\sigma = \frac{(2.0722 \times 10^{-6}\Omega^{-1})}{(7.3630 \times 10^{-4})(0.0439\ cm)}$$

$$\sigma = 6.41 \times 10^{-2} S/cm$$

So, the specific conductivity (σ) of the sample no.1 was 6.41 x 10^{-2} S/cm.

Table H4 Raw data for determination of the linear Ohmic regime and the specific conductivities of the synthesized hematite nanoparticles (cubic-like shape)

Sample	Thickness (cm)	Applied voltage (V)	Current (nA)				Specific conductivity (S/cm)
			#1	#2	#3	Avg.	
No.1	0.0493	0.130	5.14710	5.19384	5.23539	**5.19211**	1.23E-03
	0.0432	0.120	4.82093	4.85491	4.87919	**4.85167**	
	0.0400	0.110	4.61544	4.64330	4.67116	**4.64330**	
	0.0447	0.100	4.16086	4.19441	4.23216	**4.19581**	
	0.0418	0.090	3.66072	3.67912	3.70487	**3.68157**	
	0.0412	0.080	3.22795	3.25398	3.27351	**3.25181**	
	0.0434	0.070	2.93602	2.95375	2.98033	**2.95670**	
		0.060	2.43068	2.45275	2.46502	**2.44948**	
		0.050	2.18132	2.19670	2.21428	**2.19743**	
		0.040	1.71086	1.71946	1.73150	**1.72061**	
No.2	0.0338	0.130	3.93309	3.86480	3.81823	**3.87204**	9.99E-04
	0.0332	0.120	3.70832	3.59419	3.53525	**3.61259**	
	0.0375	0.110	3.26005	3.19750	3.16290	**3.20682**	
	0.0409	0.100	2.98066	2.92320	2.89395	**2.93260**	
	0.0418	0.090	2.72465	2.67203	2.63442	**2.67703**	
	0.0412	0.080	2.45465	2.43323	2.41501	**2.43430**	
	0.0381	0.070	2.19048	2.17306	2.16449	**2.17601**	
		0.060	1.90096	1.88427	1.86664	**1.88396**	
		0.050	1.61210	1.59288	1.60530	**1.60342**	
		0.040	1.31188	1.30882	1.31818	**1.31296**	
No.3	0.0338	0.130	3.05184	3.03877	2.94055	**3.01039**	7.75E-04
	0.0355	0.120	2.93704	2.78075	2.71948	**2.81242**	
	0.0329	0.110	2.64598	2.67641	2.53261	**2.61833**	
	0.0342	0.100	2.33818	2.36214	2.42330	**2.37454**	
	0.0320	0.090	2.19693	2.21921	2.17301	**2.19639**	
	0.0339	0.080	2.06953	1.97352	2.03308	**2.02538**	
	0.0337	0.070	1.80102	1.81653	1.77828	**1.79861**	
		0.060	1.69629	1.65197	1.61651	**1.65492**	
		0.050	1.45369	1.42709	1.44892	**1.44323**	
		0.040	1.33128	1.28828	1.26241	**1.29399**	
Average specific conductivity							**1.00E-03**
Standard deviation							**2.29E-04**

Note: The bold values are the average values of the data.

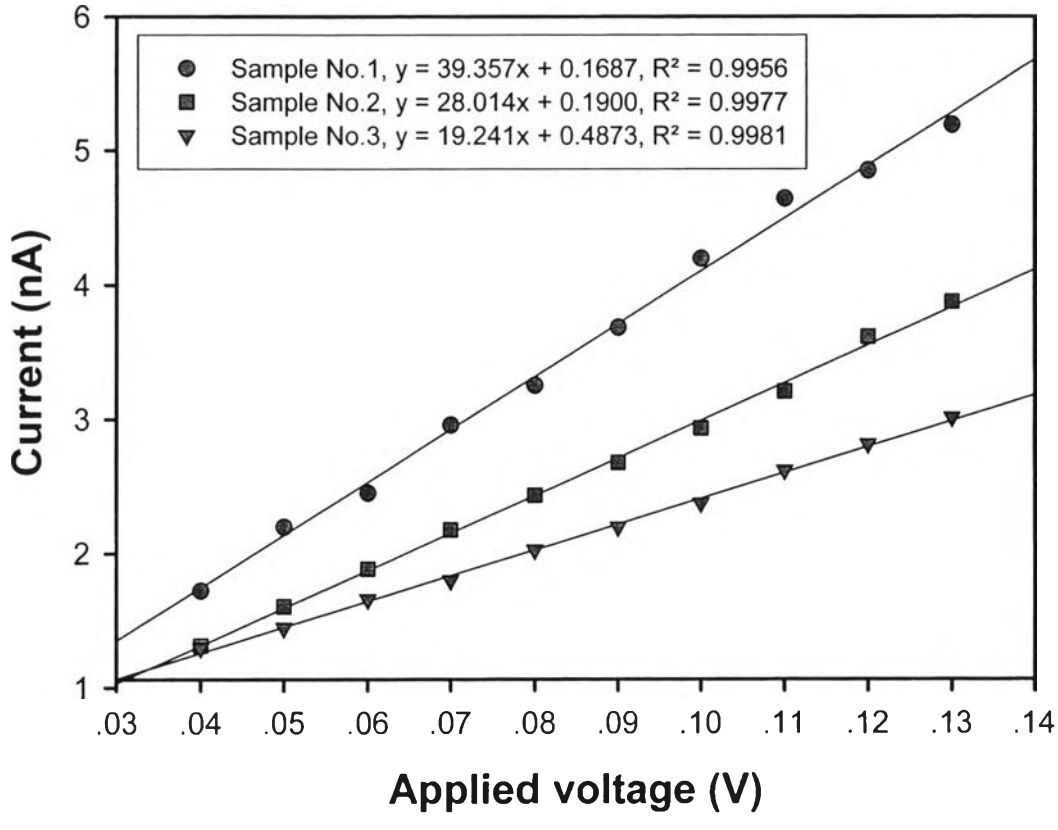

Figure H4 The linear Ohmic regime plots of the synthesized hematite nanoparticles (cubic-like shape).

Table H5 Raw data for determination of the linear Ohmic regime and the specific conductivities of the synthesized hematite nanoparticles (ellipsoidal shape)

Sample	Thickness (cm)	Applied voltage (V)	Current (nA)				Specific conductivity (S/cm)
			#1	#2	#3	Avg.	
No.1	0.0559	0.130	2.37337	2.30186	2.22207	**2.29910**	3.89E-04
	0.0608	0.120	2.18882	2.09176	2.04279	**2.10779**	
	0.0569	0.110	2.09216	2.02940	1.98689	**2.03615**	
	0.0518	0.100	1.82493	1.78870	1.75174	**1.78846**	
	0.0619	0.090	1.67464	1.61642	1.62086	**1.63731**	
	0.0526	0.080	1.53211	1.50581	1.48223	**1.50672**	
	0.0567	0.070	1.40025	1.38607	1.35335	**1.37989**	
		0.060	1.21710	1.21931	1.20921	**1.21521**	
		0.050	0.99763	0.99599	0.98989	**0.99451**	
		0.040	0.79279	0.79755	0.80758	**0.79931**	
No.2	0.0755	0.130	2.01744	1.97491	1.92081	**1.97105**	2.68E-04
	0.0705	0.120	1.81707	1.86227	1.81196	**1.83043**	
	0.0660	0.110	1.69746	1.61426	1.60916	**1.64029**	
	0.0625	0.100	1.55530	1.50130	1.47666	**1.51109**	
	0.0573	0.090	1.38622	1.35120	1.36274	**1.36672**	
	0.0605	0.080	1.25089	1.22513	1.20367	**1.22656**	
	0.0654	0.070	1.18872	1.14504	1.11636	**1.15004**	
		0.060	1.08430	1.06030	1.03829	**1.06096**	
		0.050	0.90301	0.88370	0.87945	**0.88872**	
		0.040	0.82519	0.79289	0.77377	**0.79728**	
No.3	0.0567	0.130	1.72761	1.74330	1.75725	**1.74272**	3.11E-04
	0.0514	0.120	1.58688	1.57898	1.56793	**1.57793**	
	0.0481	0.110	1.48657	1.49555	1.50452	**1.49555**	
	0.0454	0.100	1.38273	1.39388	1.40643	**1.39435**	
	0.0569	0.090	1.23590	1.22731	1.22118	**1.22813**	
	0.0482	0.080	1.13355	1.12679	1.11777	**1.12604**	
	0.0511	0.070	1.02801	1.03422	1.04353	**1.03525**	
		0.060	0.89605	0.89159	0.88357	**0.89041**	
		0.050	0.80583	0.81151	0.81800	**0.81178**	
		0.040	0.66559	0.66097	0.65766	**0.66141**	
Average specific conductivity							**3.22E-04**
Standard deviation							**6.13E-05**

Note: The bold values are the average values of the data.

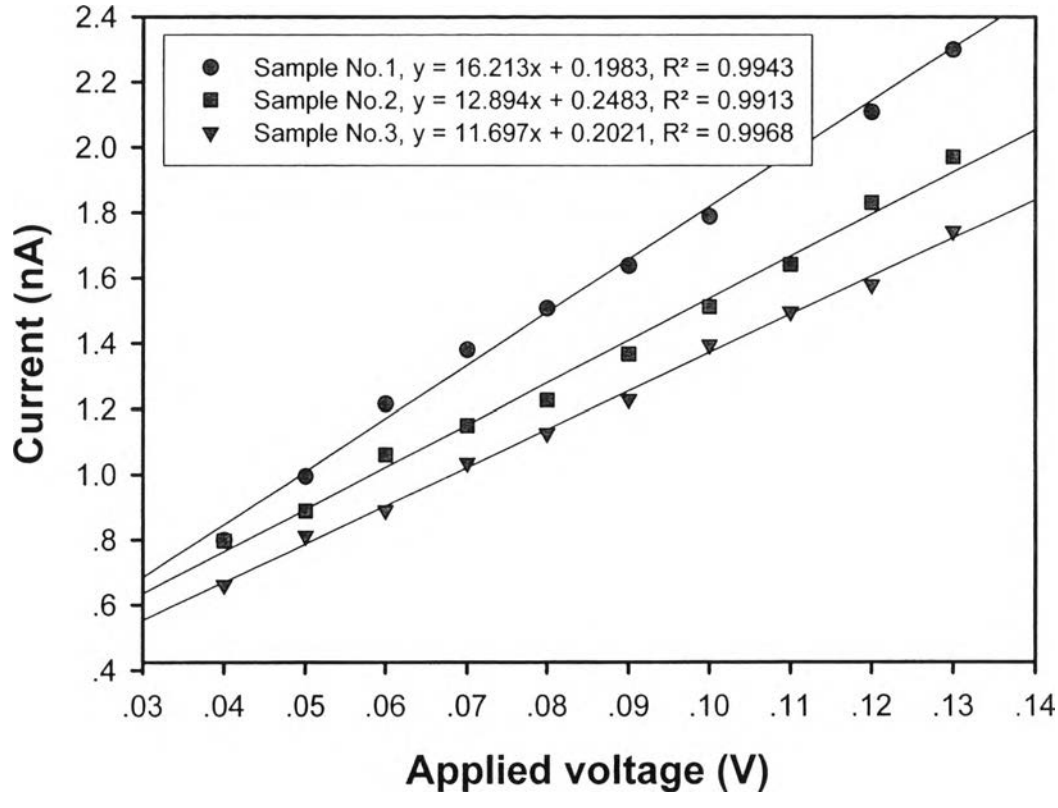

Figure H5 The linear Ohmic regime plots of the synthesized hematite nanoparticles (ellipsoidal shape).

Table H6 Raw data for determination of the linear Ohmic regime and the specific conductivities of the synthesized hematite nanoparticles (49.3 ± 8.8 nm)

Sample	Thickness (cm)	Applied voltage (V)	Current (nA)				Specific conductivity (S/cm)
			#1	#2	#3	Avg.	
No.1	0.0488	0.120	18.6343	18.3556	17.9834	**18.3245**	5.28E-03
	0.0440	0.110	17.5132	17.4993	17.4007	**17.4711**	
	0.0432	0.100	14.4205	14.8525	15.2320	**14.8350**	
	0.0438	0.090	13.0936	12.7862	12.7632	**12.8810**	
	0.0426	0.080	12.3011	12.1932	11.9648	**12.1530**	
	0.0371	0.070	10.8230	10.8551	10.8976	**10.8585**	
	0.0433	0.060	8.5292	8.8426	9.1114	**8.8277**	
		0.050	6.3366	6.3400	6.4580	**6.3782**	
		0.040	5.0352	5.0817	5.0514	**5.0561**	
		0.030	3.1725	3.3189	3.5040	**3.3318**	
No.2	0.0463	0.120	21.2392	21.4321	21.6036	**21.4250**	5.81E-03
	0.0445	0.110	19.9762	20.2176	20.1170	**20.1036**	
	0.0421	0.100	18.4354	18.3254	18.2155	**18.3254**	
	0.0464	0.090	15.4097	15.5340	15.6738	**15.5391**	
	0.0467	0.080	13.9221	13.8525	14.0195	**13.9314**	
	0.0446	0.070	12.3745	12.5492	12.4743	**12.4660**	
	0.0451	0.060	9.8964	9.9561	10.0457	**9.9661**	
		0.050	8.4136	8.3718	8.2964	**8.3606**	
		0.040	6.3985	6.4951	6.4436	**6.4457**	
		0.030	4.2399	4.2612	4.2910	**4.2640**	
No.3	0.0520	0.120	20.5446	20.7312	20.8970	**20.7243**	4.38E-03
	0.0551	0.110	18.1895	18.0990	17.9723	**18.0870**	
	0.0507	0.100	17.0078	17.2131	17.1105	**17.1105**	
	0.0627	0.090	15.0769	15.1985	15.3353	**15.2035**	
	0.0599	0.080	12.6415	12.5783	12.7300	**12.6499**	
	0.0696	0.070	11.2641	11.1740	11.3316	**11.2566**	
	0.0583	0.060	9.2231	9.3623	9.2788	**9.2880**	
		0.050	7.0467	7.1107	7.1462	**7.1012**	
		0.040	5.6385	5.5991	5.6836	**5.6404**	
		0.030	3.6069	3.5818	3.5639	**3.5842**	
Average specific conductivity							**5.16E-03**
Standard deviation							**7.20E-04**

Note: The bold values are the average values of the data.

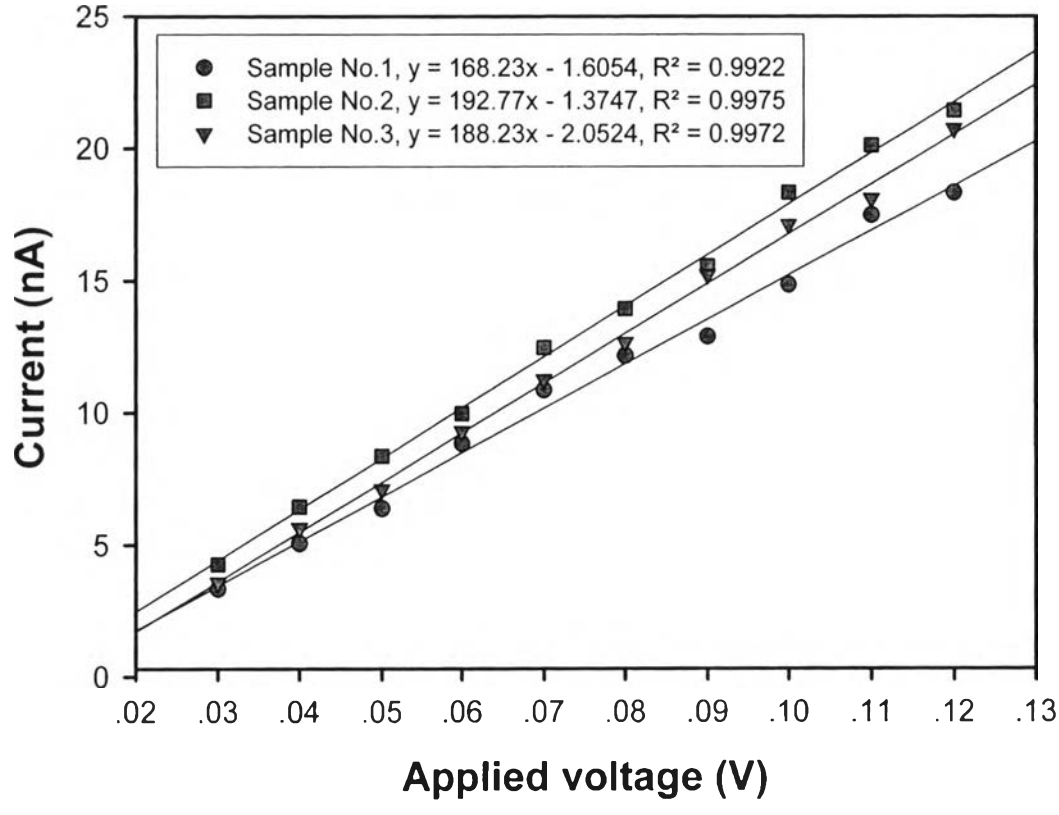

Figure H6 The linear Ohmic regime plots of the synthesized hematite nanoparticles (49.3 ± 8.8 nm).

Table H7 Raw data for determination of the linear Ohmic regime and the specific conductivities of the synthesized hematite nanoparticles (72.1 ± 15.3 nm)

Sample	Thickness (cm)	Applied voltage (V)	Current (nA)				Specific conductivity (S/cm)
			#1	#2	#3	Avg.	
No.1	0.0603	0.120	21.0612	21.1670	21.2940	**21.1741**	2.39E-03
	0.0633	0.110	19.8287	19.9886	20.1485	**19.9886**	
	0.0572	0.100	18.3613	18.2699	18.1055	**18.2456**	
	0.0600	0.090	17.9164	18.0427	18.1690	**18.0427**	
	0.0503	0.080	16.4518	16.5677	16.7168	**16.5788**	
	0.0530	0.070	15.5893	15.4656	15.3264	**15.4604**	
	0.0574	0.060	14.9008	14.9756	15.0655	**14.9806**	
		0.050	14.2783	14.1510	14.0519	**14.1604**	
		0.040	12.7137	12.7904	12.8544	**12.7862**	
		0.030	11.8085	11.7265	11.6327	**11.7226**	
No.2	0.0587	0.120	22.5587	22.6721	22.8534	**22.6947**	3.61E-03
	0.0590	0.110	20.4311	20.3294	20.1668	**20.3091**	
	0.0583	0.100	19.9580	19.8389	19.7001	**19.8323**	
	0.0545	0.090	17.8120	17.9557	18.1173	**17.9617**	
	0.0536	0.080	15.8730	15.9688	16.0806	**15.9741**	
	0.0572	0.070	15.1984	15.1077	15.0171	**15.1077**	
	0.0569	0.060	13.3674	13.4616	13.5827	**13.4706**	
		0.050	11.6662	11.6082	11.5153	**11.5966**	
		0.040	10.3713	10.4655	10.5492	**10.4620**	
		0.030	8.7284	8.7899	8.8514	**8.7899**	
No.3	0.0603	0.120	19.4778	19.3232	19.2073	**19.3361**	2.99E-03
	0.0616	0.110	17.5768	17.6652	17.7535	**17.6652**	
	0.0586	0.100	16.0944	16.2242	16.3215	**16.2134**	
	0.0571	0.090	15.5584	15.4197	15.2809	**15.4197**	
	0.0561	0.080	13.9358	13.8389	13.7420	**13.8389**	
	0.0552	0.070	12.7404	12.8173	12.8942	**12.8173**	
	0.0582	0.060	11.7348	11.6301	11.5371	**11.6340**	
		0.050	9.9426	10.0127	10.0627	**10.0060**	
		0.040	9.0740	9.0020	8.9570	**9.0110**	
		0.030	7.5141	7.4618	7.3947	**7.4569**	
Average specific conductivity							**2.99E-03**
Standard deviation							**6.13E-04**

Note: The bold values are the average values of the data.

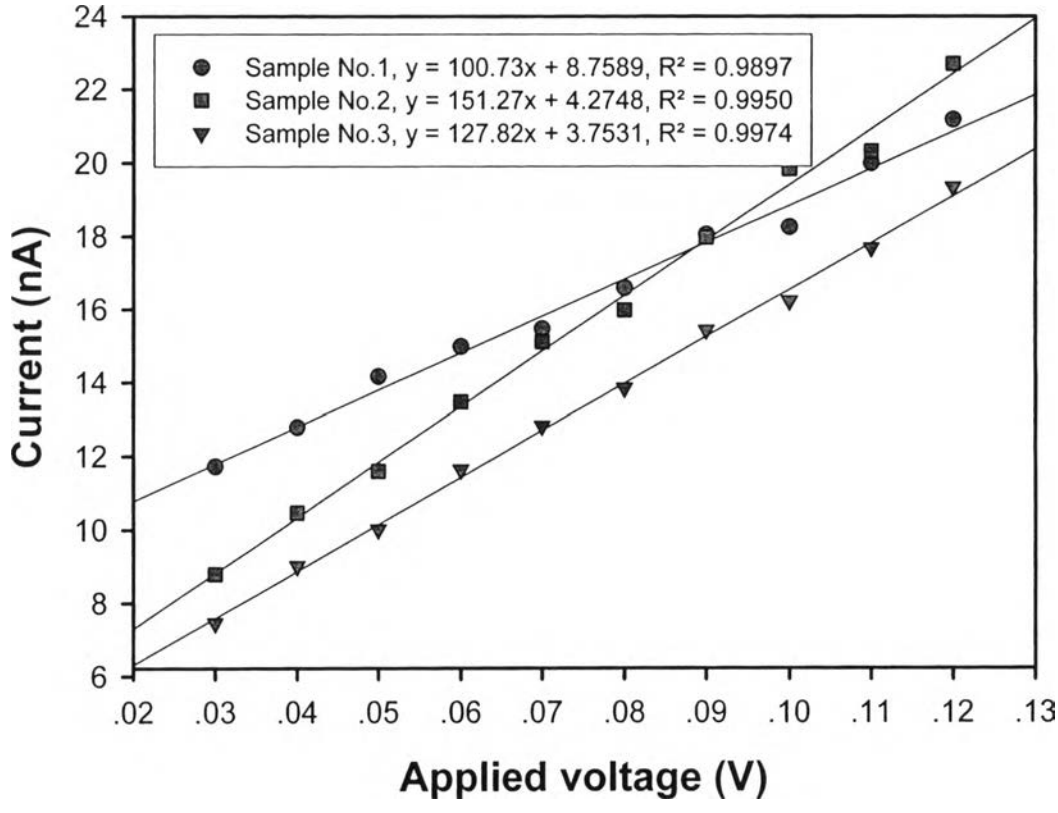

Figure H7 The linear Ohmic regime plots of the synthesized hematite nanoparticles (72.1 ± 15.3 nm).

Table H8 Raw data for determination of the linear Ohmic regime and the specific conductivities of the synthesized hematite nanoparticles (91.7 ± 15.1 nm)

Sample	Thickness (cm)	Applied voltage (V)	Current (nA)				Specific conductivity (S/cm)
			#1	#2	#3	Avg.	
No.1	0.0493	0.120	7.85913	7.88650	7.73125	**7.82562**	1.66E-03
	0.0438	0.110	7.45660	7.26050	7.10969	**7.27559**	
	0.0464	0.100	6.69955	6.45963	6.38594	**6.51504**	
	0.0486	0.090	6.07931	5.99826	5.95812	**6.01190**	
	0.0489	0.080	5.48099	5.41088	5.36965	**5.42051**	
	0.0481	0.070	4.88056	4.81187	4.79708	**4.82983**	
	0.0475	0.060	4.39019	4.31244	4.27187	**4.32483**	
		0.050	3.66432	3.65618	3.63337	**3.65129**	
		0.040	3.15764	3.12492	3.10857	**3.13038**	
		0.030	2.68845	2.65446	2.61240	**2.65177**	
No.2	0.0440	0.120	10.5651	10.1951	9.89243	**10.2175**	2.34E-03
	0.0442	0.110	9.93670	9.41729	9.17525	**9.50975**	
	0.0416	0.100	8.87391	8.43229	8.21378	**8.50666**	
	0.0422	0.090	8.17748	8.08479	7.73774	**8.00000**	
	0.0437	0.080	7.49702	7.23263	6.99389	**7.24118**	
	0.0460	0.070	6.78894	6.51199	6.45279	**6.58457**	
	0.0436	0.060	6.12046	5.86351	5.74206	**5.90868**	
		0.050	5.07717	4.91547	4.84631	**4.94632**	
		0.040	4.27584	4.18618	4.12776	**4.19659**	
		0.030	3.36336	3.29464	3.26753	**3.30851**	
No.3	0.0419	0.120	8.11175	8.15251	8.20143	**8.15523**	1.92E-03
	0.0438	0.110	7.07118	7.12821	7.18523	**7.12821**	
	0.0469	0.100	6.46550	6.43333	6.37543	**6.42475**	
	0.0495	0.090	6.06796	6.11074	6.15351	**6.11074**	
	0.0451	0.080	5.25897	5.29604	5.34371	**5.29958**	
	0.0462	0.070	4.65091	4.61400	4.57247	**4.61246**	
	0.0456	0.060	4.08691	4.10745	4.13209	**4.10882**	
		0.050	3.52535	3.49391	3.46945	**3.49624**	
		0.040	2.73964	2.75618	2.76996	**2.75526**	
		0.030	2.11449	2.09979	2.08299	**2.09909**	
Average specific conductivity							**1.97E-03**
Standard deviation							**3.46E-04**

Note: The bold values are the average values of the data.

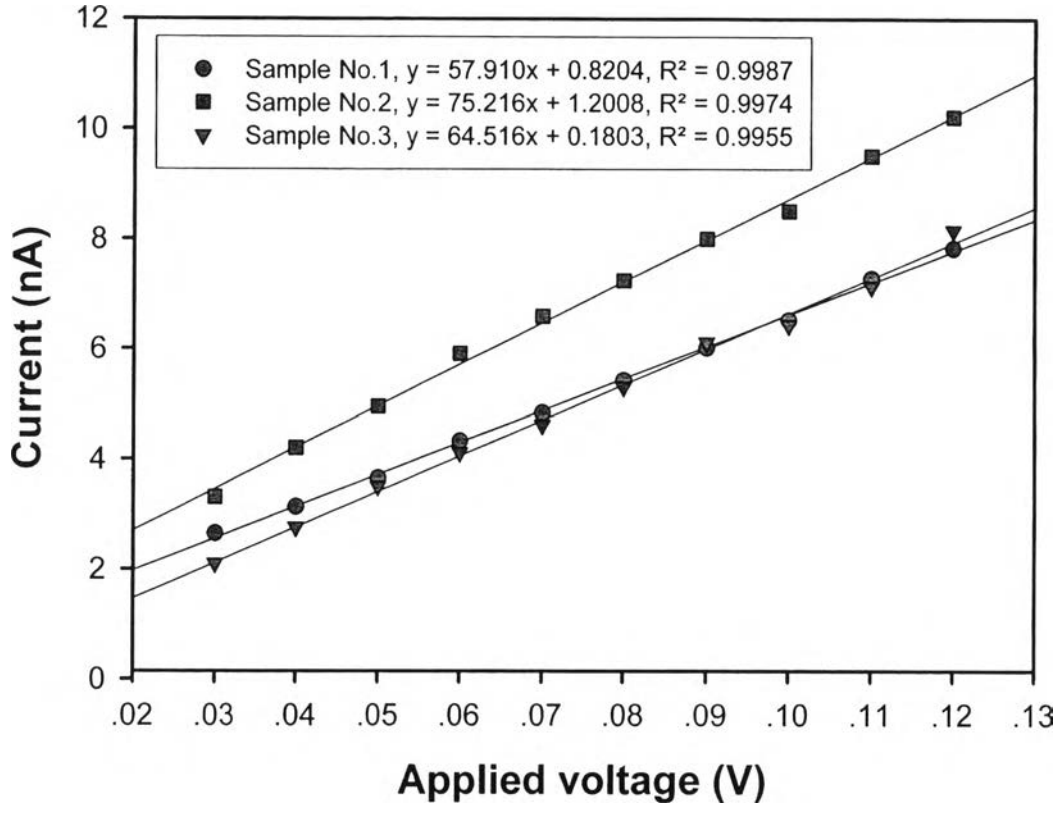

Figure H8 The linear Ohmic regime plots of the synthesized hematite nanoparticles (91.7 ± 15.1 nm).

Table H9 Raw data for determination of the linear Ohmic regime and the specific conductivities of the synthesized hematite nanoparticles (104.7 ± 20.6 nm)

Sample	Thickness (cm)	Applied voltage (V)	Current (nA)				Specific conductivity (S/cm)
			#1	#2	#3	Avg.	
No.1	0.0469	0.130	8.42951	8.47187	8.52270	**8.47469**	1.37E-03
	0.0437	0.120	7.71473	7.77695	7.83916	**7.77695**	
	0.0486	0.110	7.74637	7.70783	7.63846	**7.69755**	
	0.0473	0.100	7.12142	7.17162	7.22182	**7.17162**	
	0.0481	0.090	6.40197	6.44710	6.50512	**6.45139**	
	0.0426	0.080	6.11360	6.06508	6.01049	**6.06305**	
	0.0462	0.070	5.75855	5.78749	5.82222	**5.78942**	
		0.060	5.32136	5.27390	5.23698	**5.27741**	
		0.050	4.64592	4.67396	4.69733	**4.67241**	
		0.040	4.21682	4.18751	4.15401	**4.18611**	
No.2	0.0499	0.130	11.7712	11.8303	11.9250	**11.8422**	1.98E-03
	0.0557	0.120	10.8969	10.8427	10.7560	**10.8319**	
	0.0537	0.110	9.94438	9.88507	9.81588	**9.88178**	
	0.0503	0.100	9.34384	9.41919	9.50396	**9.42233**	
	0.0527	0.090	8.26451	8.31440	8.37260	**8.31717**	
	0.0565	0.080	7.85786	7.81100	7.76413	**7.81100**	
	0.0531	0.070	6.86501	6.91341	6.97563	**6.91802**	
		0.060	6.38926	6.35748	6.30662	**6.35112**	
		0.050	5.48739	5.53722	5.58152	**5.53538**	
		0.040	4.60488	4.63734	4.66980	**4.63734**	
No.3	0.0395	0.130	8.43810	8.37113	8.32090	**8.37671**	1.69E-03
	0.0448	0.120	7.50238	7.54008	7.57778	**7.54008**	
	0.0436	0.110	7.19472	7.25274	7.29626	**7.24790**	
	0.0383	0.100	6.66063	6.60122	6.54181	**6.60122**	
	0.0391	0.090	6.13597	6.09332	6.05067	**6.09332**	
	0.0425	0.080	5.77623	5.81110	5.84596	**5.81110**	
	0.0413	0.070	5.27847	5.23139	5.18954	**5.23313**	
		0.060	4.49180	4.52346	4.54608	**4.52045**	
		0.050	4.21828	4.18480	4.16388	**4.18899**	
		0.040	3.57870	3.55382	3.52184	**3.55145**	
Average specific conductivity							**1.68E-03**
Standard deviation							**3.03E-04**

Note: The bold values are the average values of the data.

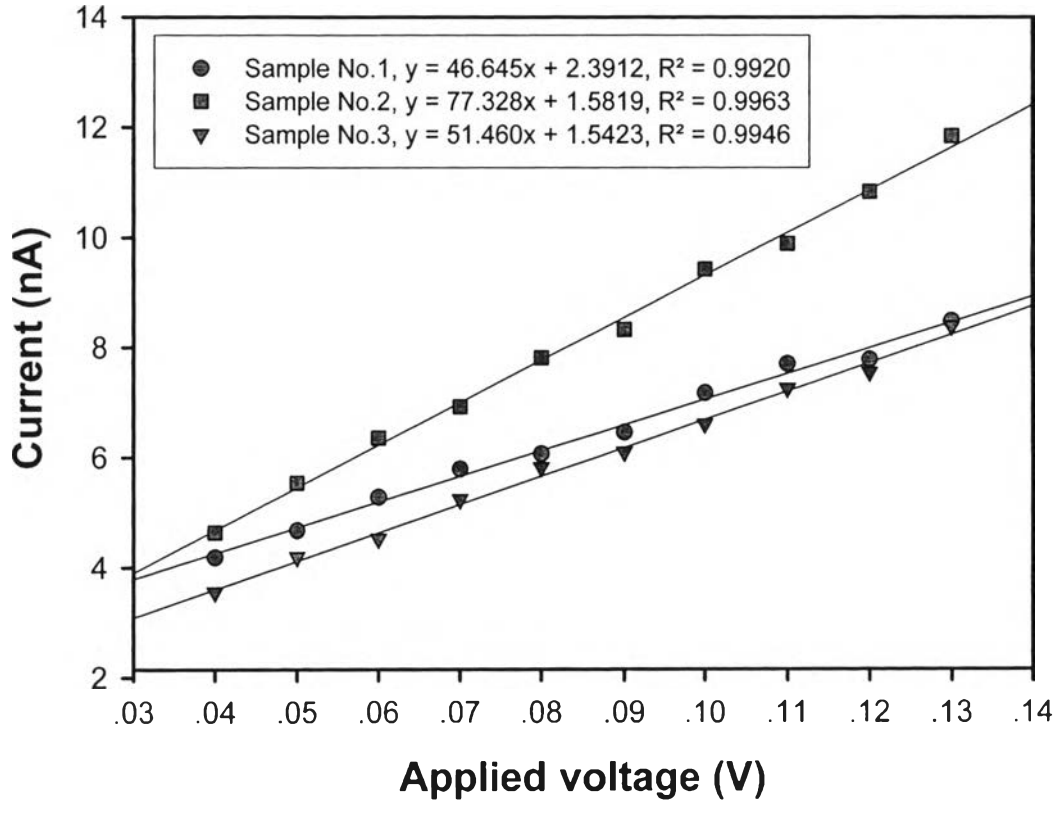

Figure H9 The linear Ohmic regime plots of the synthesized hematite nanoparticles (104.7 ± 20.6 nm).

Table H10 Raw data for determination of the linear Ohmic regime and the specific conductivities of the synthesized hematite nanoparticles (139.5 ± 28.2 nm)

Sample	Thickness (cm)	Applied voltage (V)	Current (nA)				Specific conductivity (S/cm)
			#1	#2	#3	Avg.	
No.1	0.0572	0.130	6.65398	6.49051	6.54175	**6.56208**	1.19E-03
	0.0565	0.120	6.15540	6.09432	6.07783	**6.10918**	
	0.0554	0.110	5.70160	5.78235	5.60281	**5.69559**	
	0.0546	0.100	5.04484	5.04215	4.96889	**5.01863**	
	0.0528	0.090	4.56979	4.55079	4.48303	**4.53454**	
	0.0519	0.080	4.14098	4.05509	4.02628	**4.07412**	
	0.0547	0.070	3.74573	3.68136	3.65009	**3.69239**	
		0.060	3.29546	3.27805	3.22329	**3.26560**	
		0.050	2.74649	2.70736	2.64117	**2.69834**	
		0.040	2.23681	2.25647	2.27359	**2.25563**	
No.2	0.0519	0.130	5.59573	5.50822	5.40812	**5.50403**	9.74E-04
	0.0498	0.120	5.21000	5.11544	5.10469	**5.14337**	
	0.0483	0.110	4.88972	4.75353	4.74979	**4.79768**	
	0.0477	0.100	4.50309	4.41808	4.38919	**4.43679**	
	0.0462	0.090	4.18076	4.10825	4.05539	**4.11480**	
	0.0493	0.080	3.69305	3.63709	3.60599	**3.64538**	
	0.0489	0.070	3.34951	3.31120	3.27392	**3.31154**	
		0.060	3.03337	2.97644	2.95207	**2.98729**	
		0.050	2.74071	2.67520	2.64849	**2.68813**	
		0.040	2.44601	2.42904	2.39975	**2.42493**	
No.3	0.0483	0.130	4.05069	4.07104	4.09547	**4.07240**	7.52E-04
	0.0498	0.120	3.72163	3.75164	3.78165	**3.75164**	
	0.0529	0.110	3.35229	3.33562	3.30560	**3.33117**	
	0.0535	0.100	3.16954	3.19189	3.21423	**3.19189**	
	0.0516	0.090	2.80658	2.82636	2.85180	**2.82825**	
	0.0517	0.080	2.54914	2.52891	2.50615	**2.52807**	
	0.0513	0.070	2.31755	2.32919	2.34317	**2.32997**	
		0.060	2.09103	2.07237	2.05787	**2.07376**	
		0.050	1.72934	1.73978	1.74848	**1.73920**	
		0.040	1.46347	1.45330	1.44167	**1.45282**	
Average specific conductivity							**9.72E-04**
Standard deviation							**2.20E-04**

Note: The bold values are the average values of the data.

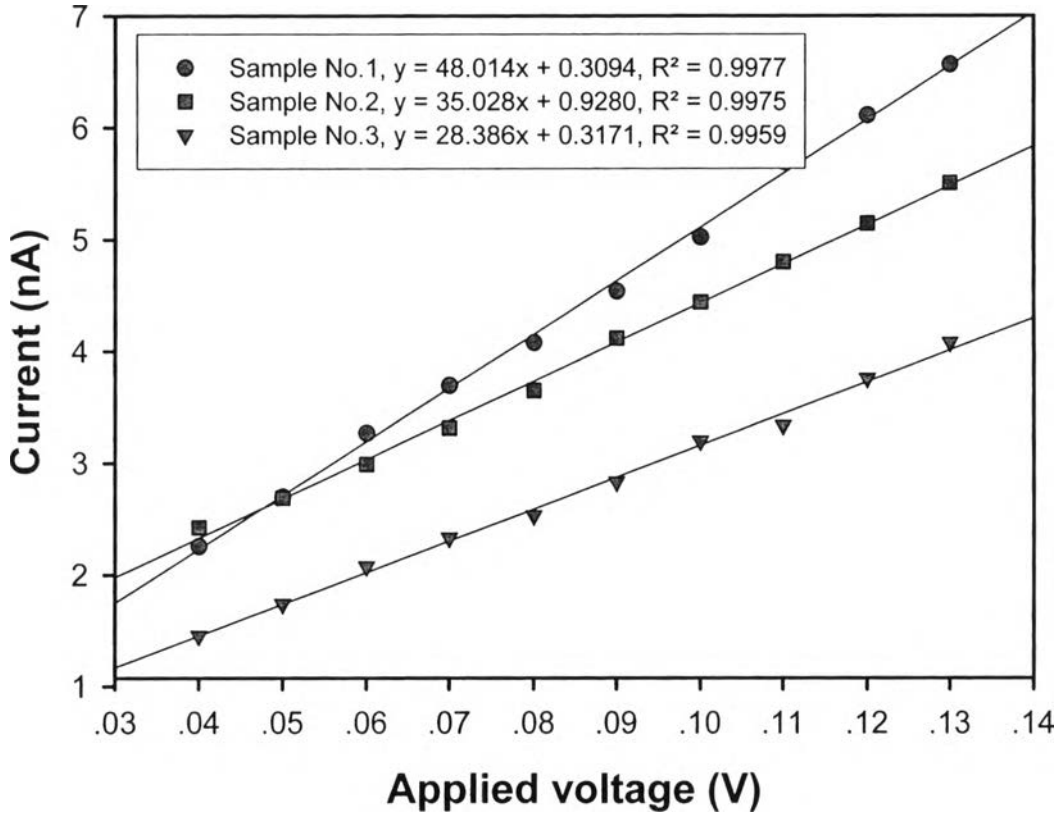

Figure H10 The linear Ohmic regime plots of the synthesized hematite nanoparticles (139.5 ± 28.2 nm).

Appendix I Magnetic Properties Measurement of the Synthesized Hematite Nanoparticles

A vibrating sample magnetometer (LakeShore, 7404), with a 4-inch electromagnet, was used to study the magnetic properties of the synthesized hematite particles. The magnetization curves were measured under the maximum magnetic field strength of 8000.0 Oe at room temperature to determine the hysteresis loops. The data were taken with a scan speed of 10 sec/point to complete the 280 points of the hysteresis loop.

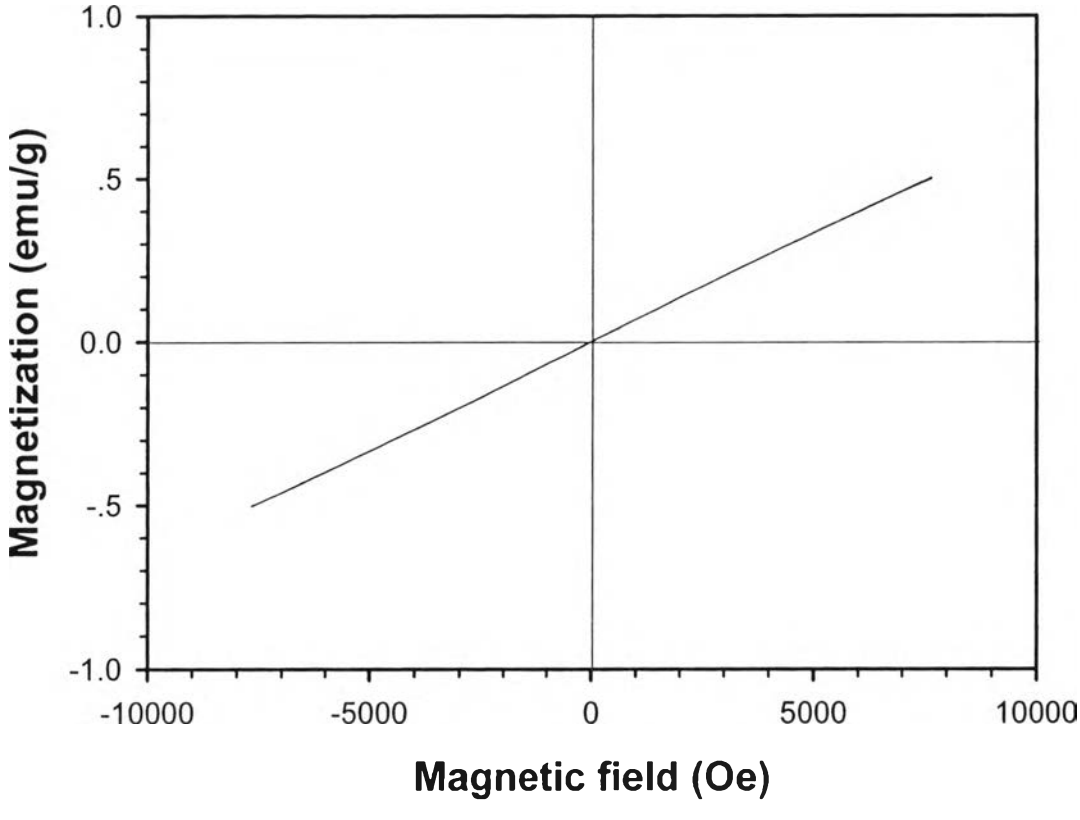

Figure I1 Room temperature magnetization curve of the 2-line ferrihydrite precursor (C = 0.3 M, and pH 7).

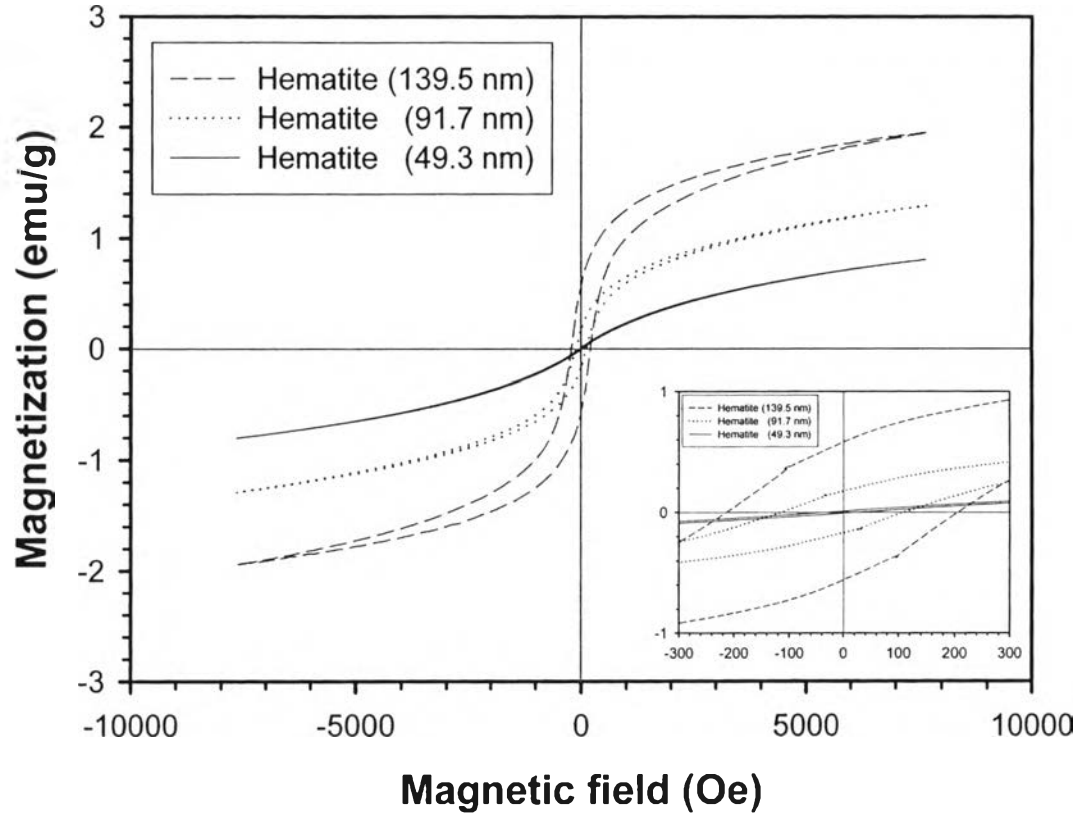

Figure I2 Room temperature magnetization curves of the synthesized hematite nanoparticles with different particle sizes.

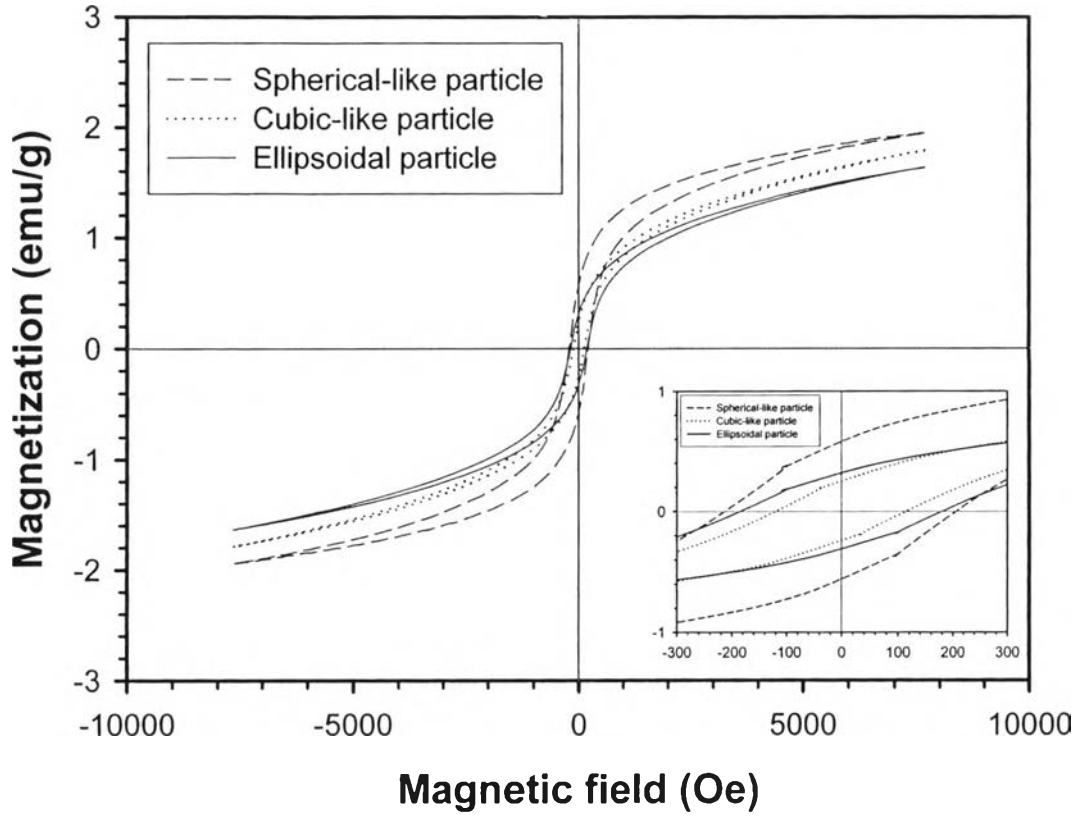

Figure I3 Room temperature magnetization curves of the synthesized hematite nanoparticles with different morphologies (dash line is the same line as represented in Figure I2).

Table 11 Summary of the magnetic parameters of the synthesized hematite nanoparticles with different particle sizes and morphologies

Sample		Magnetic parameters			
Particle shape	**Particle size (nm) ($\bar{X}$ ± SD)**	**H_c (Oe)**	**M_r (emu/g)**	**M_s (emu/g)**	**M_r/M_s**
Sphere	49.3 ± 8.8	30.2	0.00946	0.8018	0.01179
Sphere	91.7 ± 15.1	115.3	0.17104	1.2874	0.13286
Sphere	139.5 ± 28.2	211.5	0.56480	1.9433	0.29064
Cube	127.5 ± 24.3	120.2	0.24456	1.7863	0.13691
Ellipsoid	119.4 ± 44.3	185.2	0.31185	1.6332	0.19095

Note: H_c is the coercive force; M_r is the remanence magnetization (at $H = 0$ Oe); and M_s is the saturation (maximum) magnetization.

CURRICULUM VITAE

Name: Mr. Kitibodee Supattarasakda

Date of Birth: July 19, 1987

Nationality: Thai

University Education:

2006 – 2009 Bachelor Degree in Petrochemicals and Polymeric Materials, Faculty of Engineering and Industrial Technology, Silpakorn University, Nakhon Pathom, Thailand

Proceedings:

1. Supattarasakda, K.; and Sirivat, A. (2012, April 24). Synthesis and Characterization of Size-controlled Hematite (αFe_2O_3) Nanoparticles via the Chemical Precipitation Method. Proceedings of the 3rd Research Symposium on Petrochemical, and Materials Technology and the 18th PPC Symposium on Petroleum, Petrochemicals, and Polymers, Ballroom, Queen Sirikit National Convention Center, Bangkok, Thailand.

Presentation:

1. Supattarasakda, K.; and Sirivat, A. (2012, April 24). Synthesis and Characterization of Size-controlled Hematite (αFe_2O_3) Nanoparticles via the Chemical Precipitation Method. Paper presented at the 3rd Research Symposium on Petrochemical, and Materials Technology and the 18th PPC Symposium on Petroleum, Petrochemicals, and Polymers, Ballroom, Queen Sirikit National Convention Center, Bangkok, Thailand.